Defense Threat Reduction Agency
8725 John J. Kingman Road, MS 6201
Fort Belvoir, VA 22060-6201

DTRA-TR-03-31

TECHNICAL REPORT

Frequency Dependence of Q in the Crust and Upper Mantle of China and Surrounding Regions from Computations of Lg Q and the Attenuation of High-Frequency P-Waves

Approved for public release; distribution is unlimited.

May 2006

DTRA01-00-C-0213

DARE Tracking # 73777

B. J. Mitchell, et al.

Prepared by:
Saint Louis University
Department of Earth and Atmospheric Sciences
3507 Laclede Avenue
St. Louis, MO 63103

DESTRUCTION NOTICE

FOR CLASSIFIED documents, follow the procedures in DoD 5550.22-M, National Industrial Security Program Operating Manual, Chapter 5, Section 7 (NISPOM) or DoD 5200.1-R, Information Security Program Regulation, Chapter 1X.

FOR UNCLASSIFIED limited documents, destroyed by any method that will prevent disclosure of contents or reconstruction of the document.

Retention of this document by DoD contractors is authorized in accordance with DoD 5220.22M, Industrial Security manual.

PLEASE NOTIFY THE DEFENSE THREAT REDUCTION AGENCY, ATTN: IMMI, 8725 JOHN J. KINGMAN ROAD, MS-6201, FT. BELVOIR, VA 22060-6201. IF YOUR ADDRESS IS INCORRECT, IF YOU WISH IT DELETED FROM THE DISTRIBUTION LIST, OR IF THE ADDRESSEE IS NO LONGER EMPLOYED BY YOUR ORGANIZATION.

DISTRIBUTION LIST UPDATE

This mailer is provided to enable DTRA to maintain current distribution lists for reports. (We would appreciate you providing the requested information.)

- ☐ Add the individual listed to your distribution list.
- ☐ Delete the cited organization/individual.
- ☐ Change of address.

Note:
Please return the mailing label from the document so that any additions, changes, corrections or deletions can be made easily. For distribution cancellation or more information call DTRA/BDLMI (703) 767-4725.

NAME: ____________________

ORGANIZATION: ____________________

OLD ADDRESS	**NEW ADDRESS**
____________________	____________________
____________________	____________________
____________________	____________________

TELEPHONE NUMBER: ( ) ____________________

DTRA PUBLICATION NUMBER/TITLE	**CHANGES/DELETIONS/ADDITONS, etc.** *(Attach Sheet if more Space is Required)*
____________________	____________________
____________________	____________________
____________________	____________________

DTRA or other GOVERNMENT CONTRACT NUMBER: ____________________

CERTIFICATION of NEED-TO-KNOW BY GOVERNMENT SPONSOR (if other than DTRA):

SPONSORING ORGANIZATION: ____________________

CONTRACTING OFFICER or REPRESENTATIVE: ____________________

SIGNATURE: ____________________

DEFENSE THREAT REDUCTION AGENCY
ATTN: BDLMI
8725 John J Kingman Road, MS 6201
Fort Belvoir, VA 22060-6201

DEFENSE THREAT REDUCTION AGENCY
ATTN: BDLMI
8725 John J Kingman Road, MS 6201
Fort Belvoir, VA 22060-6201

REPORT DOCUMENTATION PAGE

Form Approved OMB No. 0704-0188

Public reporting burden for this collection of information is estimated to average 1 hour per response, including the time for reviewing instructions, searching existing data sources, gathering and maintaining the data needed, and completing and reviewing this collection of information. Send comments regarding this burden estimate or any other aspect of this collection of information, including suggestions for reducing this burden to Department of Defense, Washington Headquarters Services, Directorate for Information Operations and Reports (0704-0188), 1215 Jefferson Davis Highway, Suite 1204, Arlington, VA 22202-4302. Respondents should be aware that notwithstanding any other provision of law, no person shall be subject to any penalty for failing to comply with a collection of information if it does not display a currently valid OMB control number. **PLEASE DO NOT RETURN YOUR FORM TO THE ABOVE ADDRESS.**

1. REPORT DATE *(DD-MM-YYY)* May 2006	**2. REPORT TYPE** Technical Report	**3. DATES COVERED** *(From - To)*

4. TITLE AND SUBTITL Frequency Dependence of Q in the Crust and Upper Mantle of China and Surrounding Regions from Computations of Lg Q and the Attenuation of High-Frequency P-Waves (U)	**5a. CONTRACT NUMBER** DTRA 01-00-C-0213 **5b. GRANT NUMBER** **5c. PROGRAM ELEMENT NUMBER** 139E
6. AUTHOR(S) A.L. Jemberie, B.J. Mitchell, F. Leyton, R. Chu, and A. Fatehi	**5d. PROJECT NUMBER** ST **5e. TASK NUMBER** XX **5f. WORK UNIT NUMBER** DH02620
7. PERFORMING ORGANIZATION NAME(S) AND ADDRESS(ES) Saint Louis University Department of Earth and Atmospheric Sciences 3507 Laclede Avenue St. Louis, MO 63103	**8. PERFORMING ORGANIZATION REPORT NUMBER**
9. SPONSORING / MONITORING AGENCY NAME(S) AND ADDRESS(ES) Defense Threat Reduction Agency 8725 John J. Kingman Rd., MS 6201 Fort Belvoir, VA 22060-6201	**10. SPONSOR/MONITOR'S ACRONYM(S)** DTRA **11. SPONSOR/MONITOR'S REPORT NOS.** TR-03-31

12. DISTRIBUTION / AVAILABILITY STATEMENT
Approved for public release; distribution is unlimited.

13. SUPPLEMENTARY NOTES
This work was sponsored by the Defense Threat Reduction Agency under the RDT&E RMC Code B 139D R D500 ST XX 02620 25904D.

14. ABSTRACT
Starting with fundamental-mode Rayleigh-wave attenuation coefficient values predicted by previously determined frequency-independent model of shear-wave Q we have obtained frequency-dependent Q models that explain both the measured values of yr as well as of Lg coda Q and its frequency dependence at 1 Hz (Q and n respectively) for China and some adjacent regions. The process combines trial-and-error selection of a model for the depth distribution of the frequency parameter for Q with a formal inversion for the depth distribution of Q at 1 Hz. Fifteen of the derived models have depth distributions that are constant, or nearly constant, between the surface and a depth of 30 km. Distributions that vary with depth are necessary to explain the remaining seven models. Values for the depth-independent models vary between 0.4 and 0.7 everywhere except in the western portion of the Tibetan Plateau where they range between 0.1 and 0.3 for three paths. These low values lie in a region where Q and crustal Q are very low and suggest that they should also be low for high-frequency propagation. The models in which C varies with depth all show a decrease in that value ranging between 0.6 and 0.8 in the upper 15 km of the crust and (with one exception where C = 0.0) between 0.3 and 0.55 in the depth range 15 - 30 km. The distribution of highest C values (0.6 to 0.8) in the upper crust indicates that high-frequency waves will propagate most efficiently, relative to low-frequency waves, in a band that includes, and strikes north-northeastward from, the path between event 212/97 and KMI to the path between event 180/95 and station HIA in the north.

15. SUBJECT TERMS

16. SECURITY CLASSIFICATION OF:			**17. LIMITATION OF ABSTRACT**	**18. NUMBER OF PAGES**	**19a. NAME OF RESPONSIBLE PERSON**
a. REPORT Unclassified	**b. ABSTRACT** Unclassified	**c. THIS PAGE** Unclassified	SAR	42	**19b. TELEPHONE NUMBER** *(include area code)*

Standard Form 298 (Rev. 8-98)
Prescribed by ANSI Std. Z39.18

CONVERSION TABLE

Conversion Factors for U.S. Customary to metric (SI) units of measurement.

MULTIPLY ⟶ BY ⟶ TO GET
TO GET ⟵ BY ⟵ DIVIDE

angstrom	1.000 000 x E -10	meters (m)
atmosphere (normal)	1.013 25 x E +2	kilo pascal (kPa)
bar	1.000 000 x E +2	kilo pascal (kPa)
barn	1.000 000 x E -28	meter^2 (m^2)
British thermal unit (thermochemical)	1.054 350 x E +3	joule (J)
calorie (thermochemical)	4.184 000	joule (J)
cal (thermochemical/cm^2)	4.184 000 x E -2	mega joule/m^2 (MJ/m^2)
curie	3.700 000 x E +1	*giga bacquerel (GBq)
degree (angle)	1.745 329 x E -2	radian (rad)
degree Fahrenheit	$t_k = (t^o f + 459.67)/1.8$	degree kelvin (K)
electron volt	1.602 19 x E -19	joule (J)
erg	1.000 000 x E -7	joule (J)
erg/second	1.000 000 x E -7	watt (W)
foot	3.048 000 x E -1	meter (m)
foot-pound-force	1.355 818	joule (J)
gallon (U.S. liquid)	3.785 412 x E -3	meter^3 (m^3)
inch	2.540 000 x E -2	meter (m)
jerk	1.000 000 x E +9	joule (J)
joule/kilogram (J/kg) radiation dose absorbed	1.000 000	Gray (Gy)
kilotons	4.183	terajoules
kip (1000 lbf)	4.448 222 x E +3	newton (N)
kip/inch^2 (ksi)	6.894 757 x E +3	kilo pascal (kPa)
ktap	1.000 000 x E +2	newton-second/m^2 (N-s/m^2)
micron	1.000 000 x E -6	meter (m)
mil	2.540 000 x E -5	meter (m)
mile (international)	1.609 344 x E +3	meter (m)
ounce	2.834 952 x E -2	kilogram (kg)
pound-force (lbs avoirdupois)	4.448 222	newton (N)
pound-force inch	1.129 848 x E -1	newton-meter (N-m)
pound-force/inch	1.751 268 x E +2	newton/meter (N/m)
pound-force/foot^2	4.788 026 x E -2	kilo pascal (kPa)
pound-force/inch^2 (psi)	6.894 757	kilo pascal (kPa)
pound-mass (lbm avoirdupois)	4.535 924 x E -1	kilogram (kg)
pound-mass-foot^2 (moment of inertia)	4.214 011 x E -2	kilogram-meter^2 (kg-m^2)
pound-mass/foot^3	1.601 846 x E +1	kilogram-meter^3 (kg/m^3)
rad (radiation dose absorbed)	1.000 000 x E -2	**Gray (Gy)
roentgen	2.579 760 x E -4	coulomb/kilogram (C/kg)
shake	1.000 000 x E -8	second (s)
slug	1.459 390 x E +1	kilogram (kg)
torr (mm Hg, 0^0 C)	1.333 22 x E -1	kilo pascal (kPa)

*The bacquerel (Bq) is the SI unit of radioactivity; 1 Bq = 1 event/s.
**The Gray (GY) is the SI unit of absorbed radiation.

Table of Contents

Frequency Dependent Shear-wave Q Models for the Crust of China and Surrounding Regions

Alemayehu L. Jemberie and Brian J. Mitchell
Department of Earth and Atmospheric Sciences
Saint Louis University

Abstract

Starting with fundamental-mode Rayleigh-wave attenuation coefficient values (γ_R) predicted by previously determined frequency-independent models of shear-wave Q (Q_μ) we have obtained frequency-dependent Q_μ models that explain both the measured values of γ_R as well as of Lg coda Q and its frequency dependence at 1 Hz (Q_o and η respectively) for China and some adjacent regions. The process combines trial-and-error selection of a model for the depth distribution of the frequency dependence parameter (ζ) for Q_μ with a formal inversion for the depth distribution of Q_μ at 1 Hz. Fifteen of the derived models have depth distributions of ζ that are constant, or nearly constant, between the surface and a depth of 30 km. ζ distributions that vary with depth are necessary to explain the remaining seven models. ζ values for the depth-independent models vary between 0.4 and 0.7 everywhere except in the western portion of the Tibetan Plateau where they range between 0.1 and 0.3 for three paths. These low ζ values lie in a region where Q_{Lg} and crustal Q_μ are very low and suggest that they should also be low for high-frequency propagation. The models in which ζ varies with depth all show a decrease in that value ranging between 0.6 and 0.8 in the upper 15 km of the crust and (with one exception where $\zeta = 0.0$) between 0.3 and 0.55 in the depth range 15-30 km. The distribution of highest ζ values (0.6 – 0.8) in the upper crust indicates that high-frequency

waves will propagate most efficiently, relative to low-frequency waves, in a band that includes, and strikes north-northeastward from, the path between event 212/97 and KMI to the path between event 180/95 and station HIA in the north.

Introduction

Almost all mechanisms for intrinsic Q in the Earth predict that it should vary with frequency (e.g. Jackson and Anderson, 1970). The variation of Q with frequency is usually considered to vary as $Q \sim \omega^a$ where the exponent a is termed the frequency dependence parameter and may be different for different attenuating waves. In the present study we represent that parameter for shear-wave Q (Q_μ) by ζ and for Lg coda Q (Q^C_{Lg}) by η. Several studies have addressed the question of frequency dependence of Q in the mantle and have found it to be necessary for simultaneously explaining the attenuation rate of both low- and high-frequency waves. Studies have invoked frequency dependence to reconcile Q values observed for free oscillations of the Earth and 1-Hz body waves (Jeffreys, 1967; Liu et al., 1976), to explain shear-wave Q observed for ScS waves at low and high frequencies (Sipkin and Jordan, 1979), and to explain variations in Q with frequency for teleseismic P- and S-waves in the range 0.02-4.0 Hz (Der et al., 1982). Frequency dependence of Q for upper mantle material rock has also been observed in laboratory experiments (e.g. Gueguen et al., 1989; Jackson et al., 2003).

Fewer studies have addressed the question of frequency dependence for Q at crustal depths. Combined inversions of surface-wave attenuation at periods between about 5 and 50 s and of Lg coda Q at 1 Hz, have shown that Q_μ in the continental crust varies with frequency at least at frequencies of about 1 Hz and above (Mitchell, 1980; Mitchell and Xie, 1994). Determinations of Lg Q (Q_{Lg}) (e.g. Benz et al., 1997) or Lg coda Q (Q^C_{Lg}) (e.g. Xie and Mitchell, 1990a, 1990b) typically suggest the need for frequency-dependent values. It, however, has also been found possible to explain frequency-dependent Q_{Lg} or Q^C_{Lg} with a frequent-independent Q_μ model that contains a rapid increase in value at mid-crustal depths (Mitchell, 1991).

Theoretical work has shown that Q frequency dependence may be associated with intrinsic energy loss due to temperature (e.g. Gueguen, 1989) or to movements of fluid in permeable rock (e.g. O'Connell and Budiansky, 1977). Recent studies (Hammond and Humphreys, 2000; Faul et al., 2003) have concluded that the latter mechanism is not plausible at mantle depths where pressures are high, but research on this question, to our knowledge, has not yet been conducted for crustal rock at lower pressures. Some calculations, using realistic values for temperature and the frequency dependence parameter for Q, as well as assumed values for Q activation energy, suggest that temperature differences cannot explain regional differences between crustal Q values for the eastern and western United States (Mitchell, 1995). If this result is correct it suggests that regional Q variations in the upper crust are likely to be caused by regional variations in fluid content in crustal rock. Frequency dependence of Q, at least at high frequencies, may also be attributed to scattering from heterogeneities in material traversed by seismic waves (e.g. Dainty et al., 1987).

That Q varies with frequency, at least in some portions of he crust and upper mantle and over the frequency range that that relevant to seismic wave propagation over near and regional distances, appears to be well established. Consequently this frequency dependence may be of great practical consequence for magnitude determinations at near and regional distances; and in nuclear test ban treaty monitoring, for determining detection thresholds and for the implementation of methods for discriminating between earthquakes and explosions.

In this study we determine frequency dependence values (ζ) for crustal Q_μ that simultaneously explain the attenuation observed for fundamental-mode Rayleigh waves at intermediate periods (about 5-50 s) and values of Q^C_{Lg} observed in the southeastern portion of Eurasia that includes China and some adjacent regions. This will allow us to extend the applicability of previously determined frequency-independent Q_μ models determined from surface waves to higher frequencies that characterize waves recorded at near and regional distances.

Our approach differs from that used in previous surface-wave studies of Q_μ frequency dependence in that we were able, for each path, to use fundamental-mode Rayleigh-wave data and higher-frequency Lg coda data recorded by the same instrument. Earlier studies, before the widespread availability of broadband data (e.g. Mitchell, 1980) used different instruments for low- and high-frequency data. The top trace in Figure 1 shows ground motion recorded by the broadband station ULN in Mongolia for an earthquake about 530 km distant near Lake Baikal. A seismogram, if recorded by a long-period instrument of the World-Wide Standard Seismograph Stations (WWSSN), would be similar to the middle trace of Figure 1 which is obtained by low-pass filtering the upper trace at periods above 4 s. If recorded by a short-period instrument of the WWSSN the seismogram would look like the bottom trace of Figure 1 which was obtained by band-pass filtering the upper trace around 1 Hz.

Determination of Q_μ structure using fundamental-mode Rayleigh waves

Using a single-station multimode method, Jemberie and Mitchell (2003) determined three-layer frequency-independent Q_μ models for the southeastern portion of Asia that includes China and some adjacent regions. It used surface-waves that were well-recorded at surface-wave frequencies (about 5–50 s), an example of which appears in the middle trace of Figure 1. They mapped Q_μ variations for two depth ranges, 0-10 and 10-30 km and also estimated Q_μ in the depth range 30-60 km but with less reliability. They found large regional variations of Q_μ in all of the layers. Q_μ in layer 1 (the upper 10 km) varies between about 250 in southeastern China to about 40 in thoughout most of the western Tibetan Plateau. In layer 2 (10 – 30 km depth) Q_μ varies between about 140 in central and eastern China and about 60 in western Tibet and the Burma-Thailand region. The low Q_μ values in western Tibet are among the lowest found in any continental region and correlate spatially with the lowest values of Q_{Lg} ever to be reported (Xie, 2002).

In order to obtain frequency-dependent Q_μ models our process requires that we invert curves of fundamental-mode Rayleigh-wave attenuation coefficient values (γ) versus period. We did not measure these directly, but instead computed γ values for the Q_μ models of Jemberie and Mitchell (2003) along with appropriate velocity models. This computation is the first step in the inversion process described in a later section.

Lg Coda Q

Lg is usually the most prominent high-frequency phase (~0.5 Hz and higher) recorded on seismograms at regional distances in continents and can be observed at distances as great as 3000 km. Because it is so well recorded it has been used to determine magnitudes of small events at regional distances (Nuttli, 1973) and to study regional variations of attenuative properties of the crust. In stable regions it is characterized by group velocities of about 3.5 km/s and can be as low as 3.2 or 3.3 km/s in tectonically active regions.

Lg can be represented as a superposition of many higher-mode Rayleigh waves at high frequencies. Computed Lg has a relatively sharp onset followed by oscillations, or coda, that can continue for several minutes if the crustal model used for the computations contains low-velocity layers in the uppermost crust (see the bottom trace in Figure 1). The coda of observed Lg waves usually continues for a longer time than can be theoretically predicted by theoretical seismogram computations using plane-layer models. These additional oscillations are generally attributed to scattering of wave energy from crustal heterogeneities. Paradoxically, even though the coda of seismic waves is largely due to scattering, theoretical and computational work indicates that measurements of Q using coda yield values of intrinsic Q rather than scattering Q (e.g. Wennerberg, 1993). For this reason we combine surface-wave attenuation at intermediate periods (with wavelengths likely to be much longer than dimensions of heterogeneities) with Lg coda, at frequencies (near 1 Hz) that are likely to be affected by scattering, to invert for frequency-dependent models of Q_μ for the crust.

Our method for determining crustal Q_μ models is described in the following section. Those models should explain measured values for fundamental-mode Rayleigh-wave attenuation as well as average values of Q_o and η for Q_{Lg}^C along the paths of propagation. The utilization of Rayleigh-wave attenuation was discussed in the previous section. Tomographic maps of Q_o and η at 1 Hz are available for almost all of Eurasia, including our region of study (Mitchell et al., 197). The Q_o values vary between about 150 and 1000 with the lower values occurring in a broad band, the Tethysides belt, that stretches across southern Asia, including China and some adjacent regions pertinent to this study.

Method

As a first step toward determining the frequency dependence of Q_μ and how it may vary with depth in China we have developed a method by which Q_μ frequency dependence can be obtained for our crustal models using a combined forward modeling/formal inversion procedure. It is a variation of a previously developed procedure (Mitchell and Xie, 1994) and obtains a depth distributon of ζ that reconciles Q_μ values at 1 Hz with those obtained at surface-wave periods (about 5–50 s). Because simultaneous inversions for Q_μ and ζ include more parameters than do inversions for Q_μ

alone, an additional level of non-uniqueness is introduced in the models. The process proceeds as follows:

1. Compute attenuation coefficients for the fundamental Rayleigh mode, as a function of period, for the pertinent frequency-independent Q_μ models Jemberie and Mitchell (2003) and the corresponding velocity models. For our region of study we use the shear-velocity models from Jemberie (2002) except for Tibet where we used a model from Chun and Yoshi (1977).
2. Assume a depth distribution for the frequency dependence, ζ, of Q_μ and use the attenuation coefficients obtained in step 1 to obtain a Q_μ model.
3. Calculate the fundamental-mode Rayleigh-wave attenuation coefficient values which are predicted by the model obtained in step 2 and compare them with the values of step 1. An example appears in Figure 2. If they agree within reasonable uncertainties go to step 4; if not, try a new distribution of ζ.
4. From the results of step 3, compute Q_μ at frequencies of interest (1 Hz for the present study). Figure 3 shows an example of 1Hz Q_μ models computed using five different ζ distributions, assumed to be constant with depth, for a path between station BRVK and an event that occurred on day 325 of the year 1988 (325/98 in Figures 5 and 6).
5. Compute synthetic Lg seismograms (Figure 4) at several distances from a seismic source using the appropriate velocity and Q_μ models from step 2.
6. Apply the stacked spectral ratio (SSR) method of Xie and Nuttli (1988) to the set of synthetic seismograms in step 4 to obtain values of Q_o and η predicted by the derived Q_μ model and compare them to the measured values from maps of (Mitchell et al., 1997) in Figures 5 and 6.
7. If necessary, change the depth distribution of ζ in step 2 and repeat the procedure.

Table 1 shows derived Q_o and η values for five different ζ values for a path between event 325/98 and station BRVK. Values of both Q_o and η increase as the value of ζ increases. Comparison of Q_o values in Table 1 with Figure 5 shows that the best value of ζ that can predict Q_o lies between 0.4 and 0.6. We found (Figure 7d) that a ζ value of 0.55 best predicts the value of Q_o observed for that path (647 ± 51) and also predicts the

η value of 0.37 ± 0.03 This value is lower than the average ζ value (about 0.5 on average) for the path in Figure 6. In cases, such as this, where Q_o and η cannot both be fit precisely, we assume that Q_o is more likely to be measured more accurately than η. η values may be inaccurate because they are obtained by differencing values of Q at two different frequencies.

Results

The frequency-dependent models obtained using the above procedure appear in Figures 7a-d. The solid lines on the left-hand side of each pair of boxes are frequency-independent Q_μ models obtained using the single-station multimode method (Jemberie and Mitchell, 2003) and the dashed lines show models at 1 Hz using our procedure for obtaining Q_μ frequency dependence. The boxes on the right-hand side of each pair show the assumed distributions of ζ with depth. For 15 of the 22 models, a constant value of ζ, or a distribution that varies with depth by no more than 0.05, produced acceptable results. Values for these models range between 0.4 and 0.7 everywhere in the region of study except the western portion of the Tibetan Plateau where values lie in the range 0.1 – 0.3. One path, 284/94 to LSA in the eastern portion of the Tibetan Plateau has a ζ value 0.45 which is intermediate between values for paths in the western part of the plateau and paths outside, and to the east of, the plateau.

The remaining seven models require that ζ values at depths greater than 15 km be smaller those in the upper 15 km of the crust. For the upper 15-km thick layer ζ ranges between 0.6 and 0.8, and for greater depths ranges (with one exception) between 0.3 and 0.55. The exceptional value is 0.0. Values of Q_o and η for Lg attenuation at 1 Hz predicted by the models appear with each pair of panels. Note that, as shown by the model in the upper left of Figure 7a, a model with a nearly frequency-independent Q_μ can still produce a frequency-dependent Q_{Lg} value if Q_μ increases rapidly with depth at mid-crustal depths. This phenomenon was shown to occur in the crust of the Basin and Range province in the western United States (Mitchell, 1991).

The low values for ζ in the western Tibetan Plateau coincide with very low values of Q_μ found in the crust of this region using multimode surface waves (Jemberie and

Mitchell, 2003), as well as with very low Q_{Lg} values at 1-Hz frequencies (Xie, 2003). These results indicate that surface-waves at periods of ~5–50 s as well as Lg or Lg coda at 1 Hz, and probably higher frequencies, propagate less efficiently in western Tibet than anywhere else in our region of study. The rates of attenuation in this region for both surface-wave periods (~5-50 s) and Lg frequencies (~about 1 Hz) are the highest so far measured for any continental region. An early study of Q in the central Tibetan Plateau (Chang and Yao, 1979), using spectral rations of S and ScS waves, found a Q value of about 25 that must pertain predominantly to upper mantle depths.

An interpretation of our results in terms of a continuous relaxation model for the crust would indicate that the relaxation spectrum (Q_μ^{-1}) is shifted to higher frequencies compared to other parts of our region of study, an effect that could be produced by higher temperatures or elevated levels of tectonic stress. Sublithospheric mantle heat flow estimated by Artemieva and Mooney (2001) is elevated throughout the western and central parts of the Tibetan Plateau relative to surrounding regions. It is probably pertinent that electrical resistivity values at mid- and lower-crustal depths are very low there (Wei et al., 2001), suggesting the presence of melt or fluids that may been released by hydrothermal reactions initiated by the high temperatures.

Conclusions

We have obtained frequency-dependent models of Q_μ that explain the variation of fundamental-mode Rayleigh-wave attenuation coefficients with period predicted by the Q_μ models of Jemberie and Mitchell (2003) as well as previously mapped values of Q_o and η in China and some adjacent regions. ζ values for depth-independent models vary between 0.4 and 0.7 through most of the region of study, but range between 0.1 and 0.3 in the western portion of the Tibetan Plateau. The latter (low) ζ values coincide with regions where Q_{Lg} and crustal Q_μ were previously reported to be very low and indicate that high-frequency propagation should also be low compared to other regions. The models in which ζ varies with depth all show a decrease in that value ranging between 0.6 and 0.8 in the upper 15 km of the crust and between 0.3 and 0.55 (with one exceptionally value) in the depth range 15-30 km. The distribution of highest ζ values (0.6 – 0.8) in the upper crust indicates that high-frequency waves will propagate most efficiently, relative to low-frequency waves, in a band that includes, and strikes north-northeastward from, the path between event 212/97 and KMI to the path between event 180/95 and station HIA in the north.

Our results indicate that wave propagation at surface-wave periods (~5–50 s), at 1 Hz, and probably higher frequencies, are less efficient in western Tibet than anywhere else in our region of study and that the region is characterized by the least efficient propagation of seismic waves, at all seismic frequencies, yet known for any continental region. The low ζ values can be explained if wave propagation in the crust of this region can be characterized by a continuous relaxation model that has been displaced to higher frequencies by temperatures and/or tectonic stress levels that are higher than they are in surrounding regions.

Acknowledgments

We thank Lianli Cong for providing his code for plotting crustal Q models and Robert Herrmann for writing the mode summation code for computing Lg synthetics used in this study. Our work benefited from helpful discussions Jack Xie at Lamont-Doherty Geological Observatory. This research was sponsored by the Defense Threat Reduction Agency Contract No. DTRA-01-00-C-0213.

References

Artemieva, I.M., and W.D. Mooney (2001), *Thermal thickness and evolution of Precambrian lithosphere: A global study,* J. Geophys. Res., *106*, 16387-16414.

Benz, H.M., A. Frankel and D.M. Boore (1997), *Regional Lg attenuation for the continental United States*, Bull. Seism. Soc. Am., *87*, 606-619.

Chang, L., and Z. Yao (1979), *The Q-value of the medium of the Tibetan Plateau around Lasa region*, Acta Geophys. Sinica, *22*, 299-303.

Chun, K., and T. Yoshii (1977), *Crustal structure of the Tibetan Plateau: A surface wave study by a moving window analysis*, Bull. Seism. Soc. Am., *67*, 735-750.

Dainty, A.M., R.M. Duckworth and A. Tie (1987), *Attenuation and backscattering from local coda*, Bull. Seism. Soc. Am., *77*, 1728-1747.

Der, Z.A., T.W. McElfresh, and A. O'Donnell (1982), *An investigation of the regional variations and frequency dependence of anelastic attenuation of the mantle under the United States in the 0.5-4 Hz band*, Geophys. J. Roy. Soc., *69*, 67-99.

Faul, U.H., J. D. Fitz Gerald and I. Jackson, *Shear-wave attenuation and dispersion in melt-bearing olivine polycrystals II. Microstructural interpretation and seismological implications*, J. Geophy. Res., in press, 2003.

Gueguen, Y., M. Darot, P. Mazot and J. Woirgard (1989), *Q^{-1} of forsterite single crystals*, Phys. Earth Planet. Inter., *55*, 254-258.

Hammond, W.C., and E.D. Humphreys (2000), *Upper mantle seismic wave velocity: Effects of realistic partial melt geometries*, J. Geophys. Res., *105*, 10975-10986.

Jackson, I., U.H. Faul, J.D. Fitz Gerald and B.H. Tan (2003), *Shear-wave attenuation and dispersion in melt-bearing olive polycrystals I. Specimen fabrication and mechanical testing*, J. Geophys. Res., in press.

Jackson, D.D., and D.L. Anderson (1970), *Physical mechanisms for seismic wave attenuation*, Rev. Geophys., *8*, 1-63.

Jeffreys, H. ((1967), *Radius of the Earth's core*, Nature, *215*, 1365-1366.

Jemberie, A.L. (2002), *Shear-wave attenuation and velocity studies in southeastern Asia*, Ph.D. Diss., Saint Louis University, St. Louis, Missouri, USA, 218 pp.

Jemberie, A.L., and B.J. Mitchell (2003), *Shear-wave Q structure and its lateral variation in the crust of China and surrounding regions*, Geophys. J. Int., submitted.

Liu, H.P., D.L. Anderson, and H. Kanamori (1976), *Velocity dispersion due to anelasticity: Implications for seismology and mantle composition*, Geophys. J. Roy. Soc., *47*, 41-58.

Mitchell, B.J. (1980), *Frequency dependence of shear wave internal friction in the continental crust of eastern North America*, J. Geophys. Res., *85*, 5212-5218.

Mitchell, B.J. (1991), *Frequency dependence of Q_{Lg} and its relation to crustal anelasticity in the Basin and Range province*, Geophys. Res. Lttrs., *18*, 621-624.

Mitchell, B.J. (1995), *Anelastic structure and evolution of the continental crust and upper mantle from seismic surface wave attenuation*, Rev. Geophys., *33*, 441-462.

Mitchell, B.J., and J. Xie (1994), *Attenuation of multiphase surface waves in the Basin and Range Province – III. Inversion for crustal anelasticity*, Geophys. J. Int., *116*, 468-484.

Mitchell, B.J., Y. Pan, J. Xie and L. Cong (1997), *Lg coda Q variation across Eurasia and its relation to crustal evolution*, J. Geophys. Res., *102*, 22767-22779.

Nuttli, O.W. (1973), *Seismic wave attenuation and magnitude relations for eastern North America*, J. Geophys. Res., *78*, 876-885.

O'Connell, R.J., and B. Budiansky (1977), *Viscoelastic properties of fluid –saturated cracked solids*, J. Geophys. Res., *82*, 5719-5735.

Sipkin, S.A., and T.H. Jordan (1979), *Frequency dependence of Q_{ScS}*, Bull. Seism. Soc. Am., *69*, 1055-1079.

Wei, W., M. Unsworth, A. Jones, J. Booker, H. Tan, D. Nelson, L. Chen, S. Li, K. Solon, P. Bedrosian, S. Jin, M. Deng, J. Ledo, D. Kay, and B. Roberts (2001), *Detection of widespread fluids in the Tibetan crust by magnetotelluric studies*, Science, *292*, 716-718.

Wennerberg, L. (1993), *Multiple-scattering interpretations of coda-Q measurements*, Bull. Seism. Soc. Am., *83*, 279-290.

Xie, J. (2002), *Lg Q in the eastern Tibetan Plateau*, Bull. Seism. Soc. Am., *92*, 871-876.

Xie, J., and O.W. Nuttli (1988), *Interpretation of high-frequency coda at large distances: Stochastic modeling and method of inversion*, Geophys. J., *95*, 579-595.

Xie, J., and B.J. Mitchell (1990a), *A back-projection method for imaging large-scale lateral variations of Lg coda Q with application to continental Africa*, Geophys. J. Int., *100*, 161-181.

Xie, J., and B.J. Mitchell (1990b), *Attenuation of multiphase surface waves in the Basin and Range province, I, Lg and Lg coda*, Geophys. J. Int., *102*, 121-137.

Table Caption

Table 1. Lg Q at 1 Hz (Qo) and frequency dependence (η) values derived from the stacked spectral ratios (Xie and Nuttli, 1988) of the synthetic seismograms obtained using the 1-Hz shear-wave Q (Q_μ) structure and its frequency dependence (ζ) for the path between event 325/98 and station BRVK. The numbers in column for F give the frequency ranges utilized in the determinations.

Figure Captions

Figure 1. Vertical-component seismogram recorded by the broadband instrument at station ULN for an earthquake that occurred on 30 June 1995 at an epicentral distance of about 530 km. The top trace shows the original broadband ground motion, the middle trace is the original record after it has been low-pass filtered for frequencies below 0.25 Hz (periods above 4 s), and the bottom trace is the original record after it has been band-pass filtered around 1 Hz.

Figure 2. Comparison of Rayleigh-wave attenuation coefficients predicted by the three-layer frequency-independent model of Q_μ with a frequency-dependent model for spectra obtained at station ULN for event 180/95. The necessary ζ values are 0.65 for depths between 0 and 15 km and 0.60 for depths greater than 15 km.

Figure 3. 1-Hz Q_μ models computed using five different values of Q_μ frequency dependence (ζ).

Figure 4. Synthetic Lg seismograms generated using the Q_μ structure obtained at 1 Hz and the velocity model for a subregion of China.

Figure 5. Topographic map of Lg coda Q at 1 Hz (Q_o) for most Eurasia (modified from Mitchell et al., 1997) showing paths between events and stations where frequency-independent models of Q_μ structure were determined by Jemberie and Mitchell (2003).

Figure 6. Tomographic map of the frequency dependence (η) of Lg coda Q at 1 Hz for most of Eurasia (modified from Mitchell et al., 1997) showing paths between events and stations.

Figure 7a. Frequency-dependent models of Q_μ structure for Tibet and the southernmost portion of the study area. The solid line in left-hand panels for each path presents frequency-independent Q_μ models that explain measured Rayleigh-wave attenuation at periods between about 5 and 50 s. The model delineated by the dashed line shows a Q_μ model at 1 Hz that explains both fundamental-mode Rayleigh-wave attenuation and measured Lg coda Q values at 1 Hz. The caption identifies the recording station and date of the event and gives values for Lg Q and its frequency dependence at 1 Hz that are predicted by the 1-Hz Q_μ model. The right-hand panel shows the depth distribution of Q_μ frequency-dependence that explains the two models on the left. The caption in this panel gives the value of ζ for the upper 15 km of the model (first number) and for the depth range between 15 and 60 km (second number).

Figure 7b. Frequency-dependent models of Q_μ structure for central and western China, Mongolia and peripheral regions. See the caption for Figure 7a for an explanation of the models and symbols.

Figure 7c. Frequency-dependent models of Q_μ structure for paths in northern China, Mongolia and portions of southern Siberia. See the caption for Figure 7a for an explanation of the models and symbols.

Figure 7d. Frequency-dependent models of Q_μ structure for the western portion of the study area. See the caption for Figure 7a for an explanation of the models and symbols.

Table 1

ζ	Qo	η	Frequency Range
0.0	117±14	0.068±0.266	0.09 – 2.0
0.2	224±12	0.172±0.027	0.8 – 4.0
0.4	399±22	0.326±0.024	0.9 – 5.0
0.6	762±76	0.387±0.040	0.8 – 5.0
0.8	837±282	0.833±0.189	2.0 – 6.0

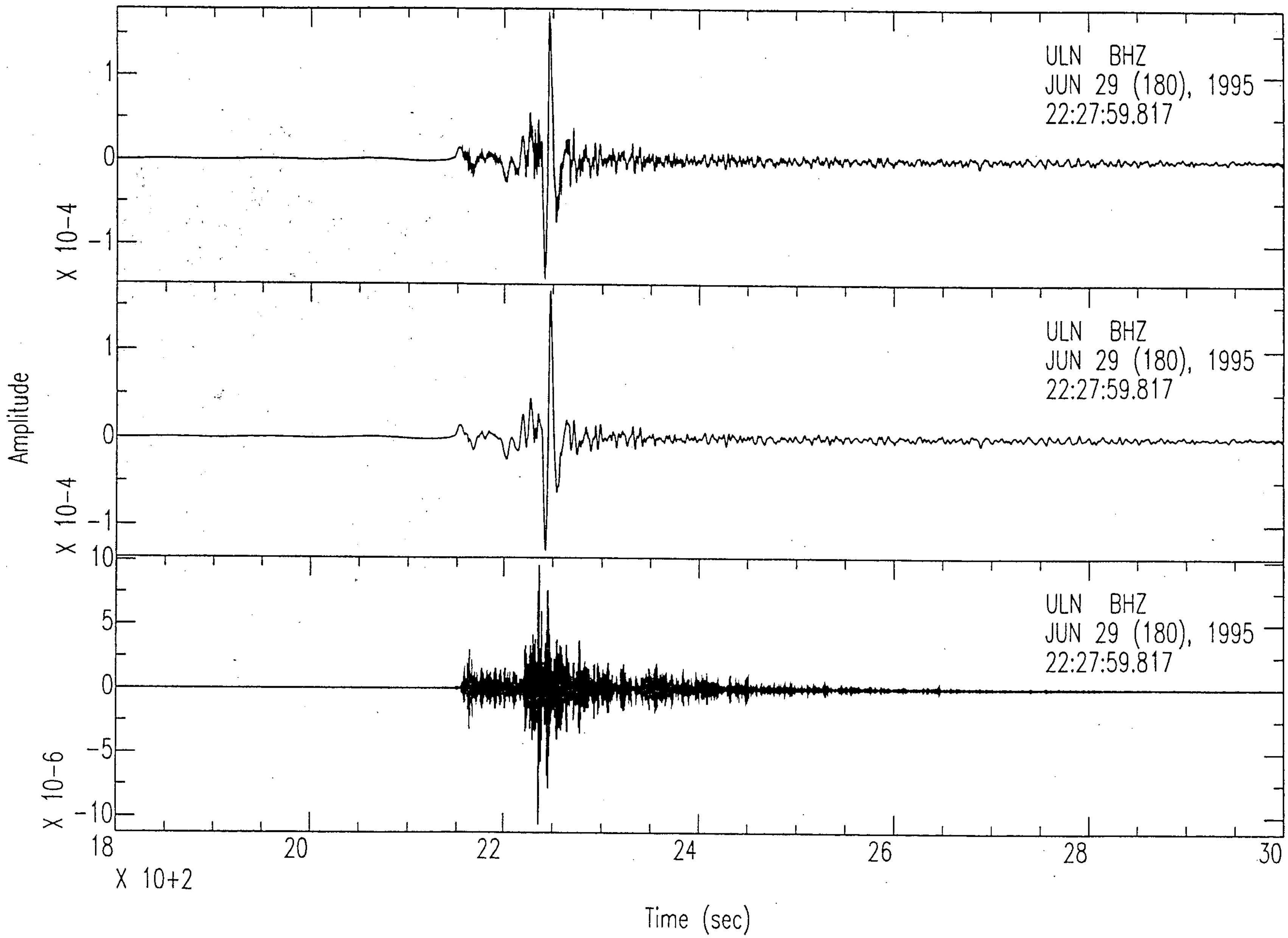
ULN BHZ
JUN 29 (180), 1995
22:27:59.817
ULN BHZ
JUN 29 (180), 1995
22:27:59.817
ULN BHZ
JUN 29 (180), 1995
22:27:59.817
Amplitude
X 10−4
X 10−4
X 10−6
X 10+2
Time (sec)

Figure 1

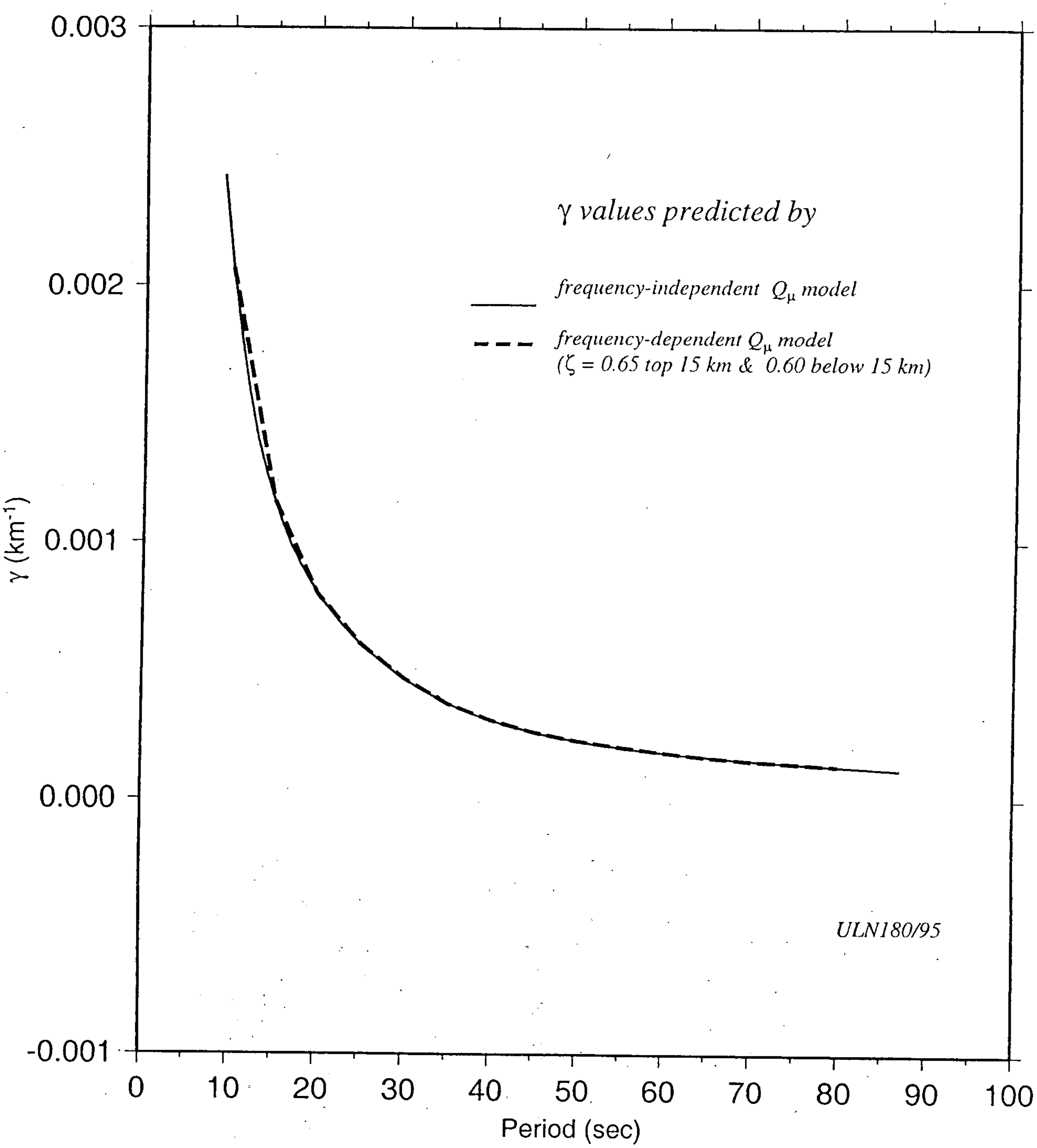
0.003
0.002
0.001
0.000
-0.001
γ (km-1)
γ values predicted by
frequency-independent Qμ model
frequency-dependent Qμ model
(ζ = 0.65 top 15 km & 0.60 below 15 km)
ULN180/95
0
10
20
30
40
50
60
70
80
90
100
Period (sec)

Figure 2

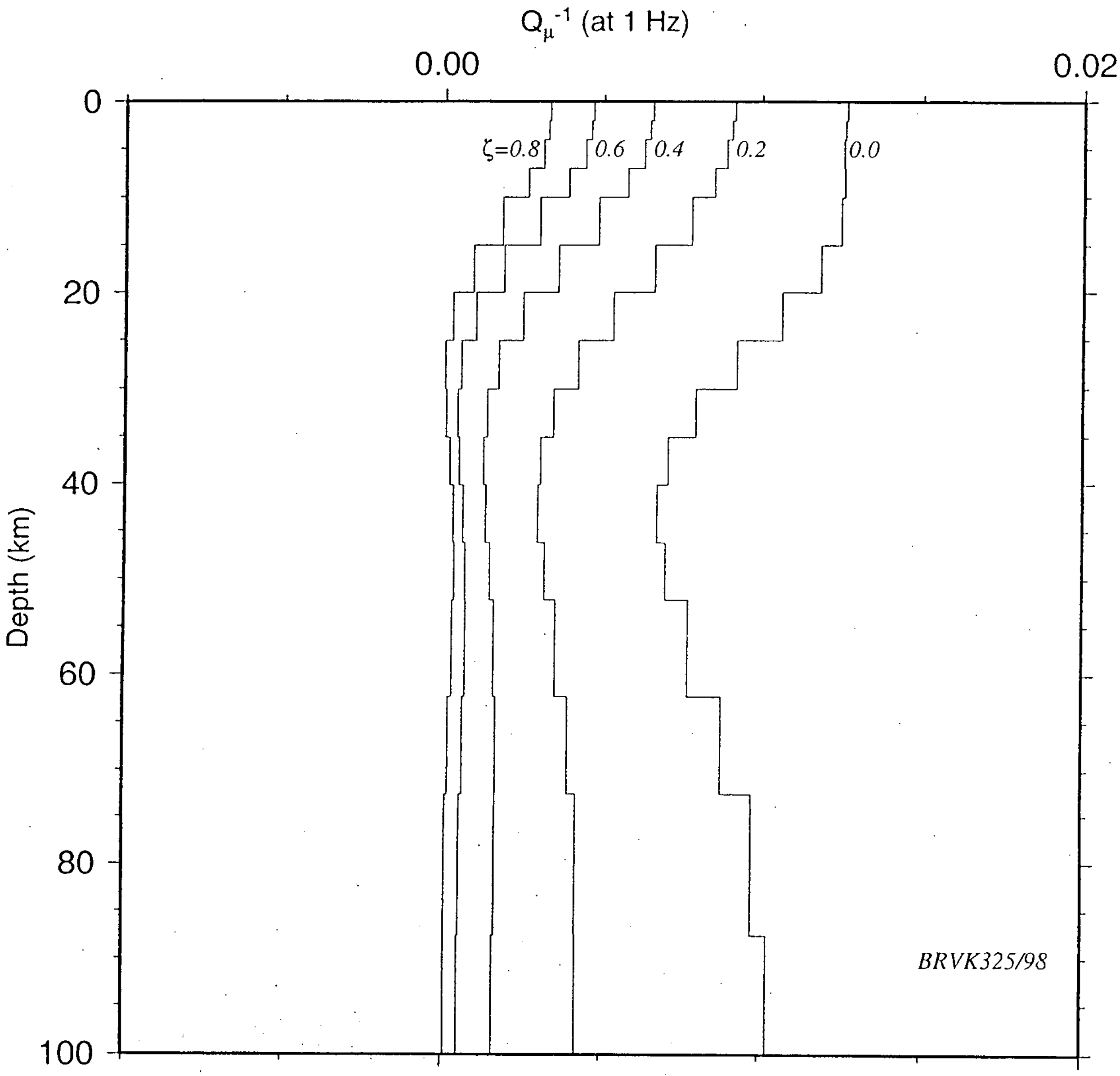

Q_μ^{-1} (at 1 Hz)
0.00
0.02
0
20
40
60
80
100
Depth (km)
ζ=0.8
0.6
0.4
0.2
0.0
BRVK325/98

Figure 3

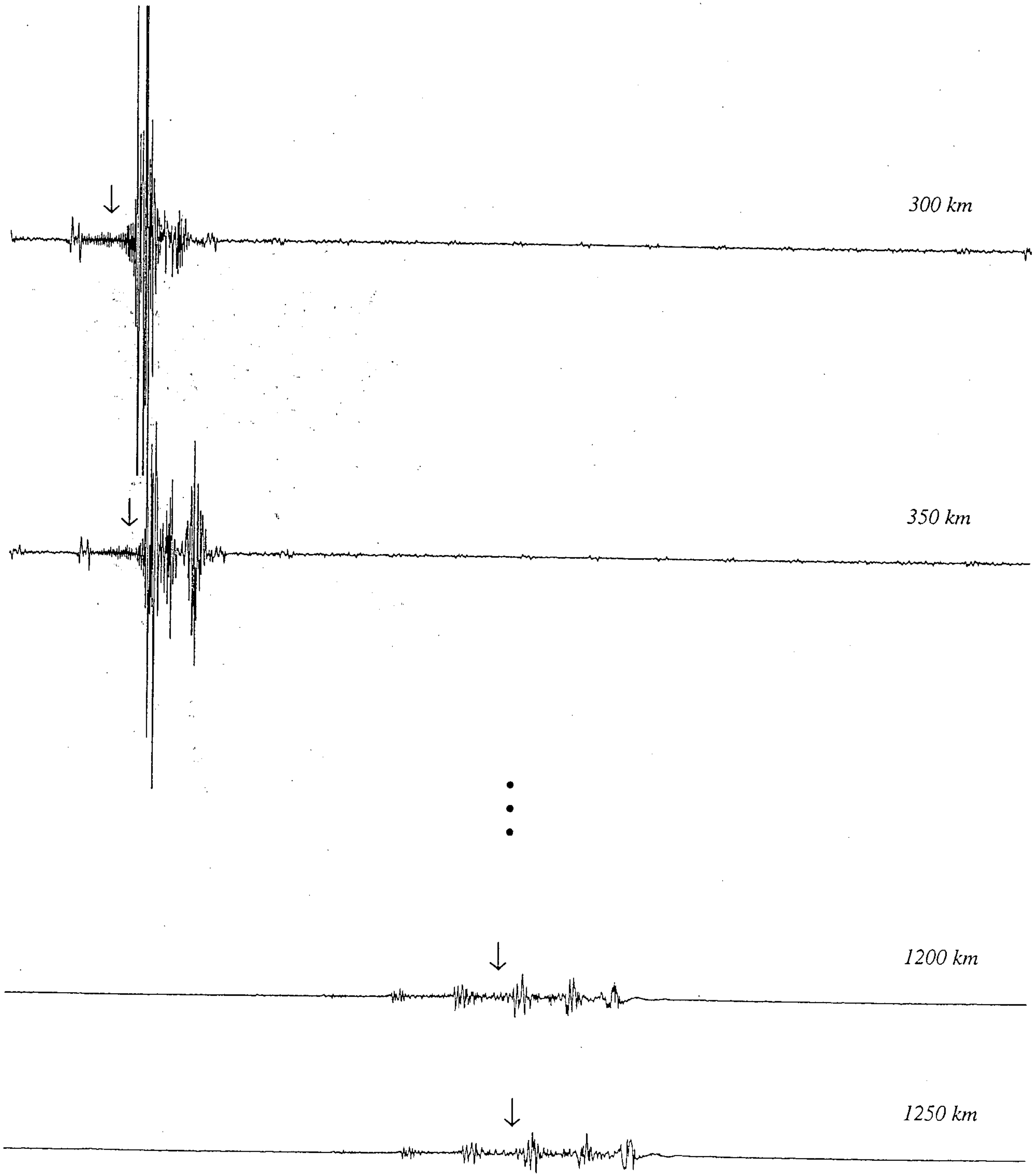

Figure 4

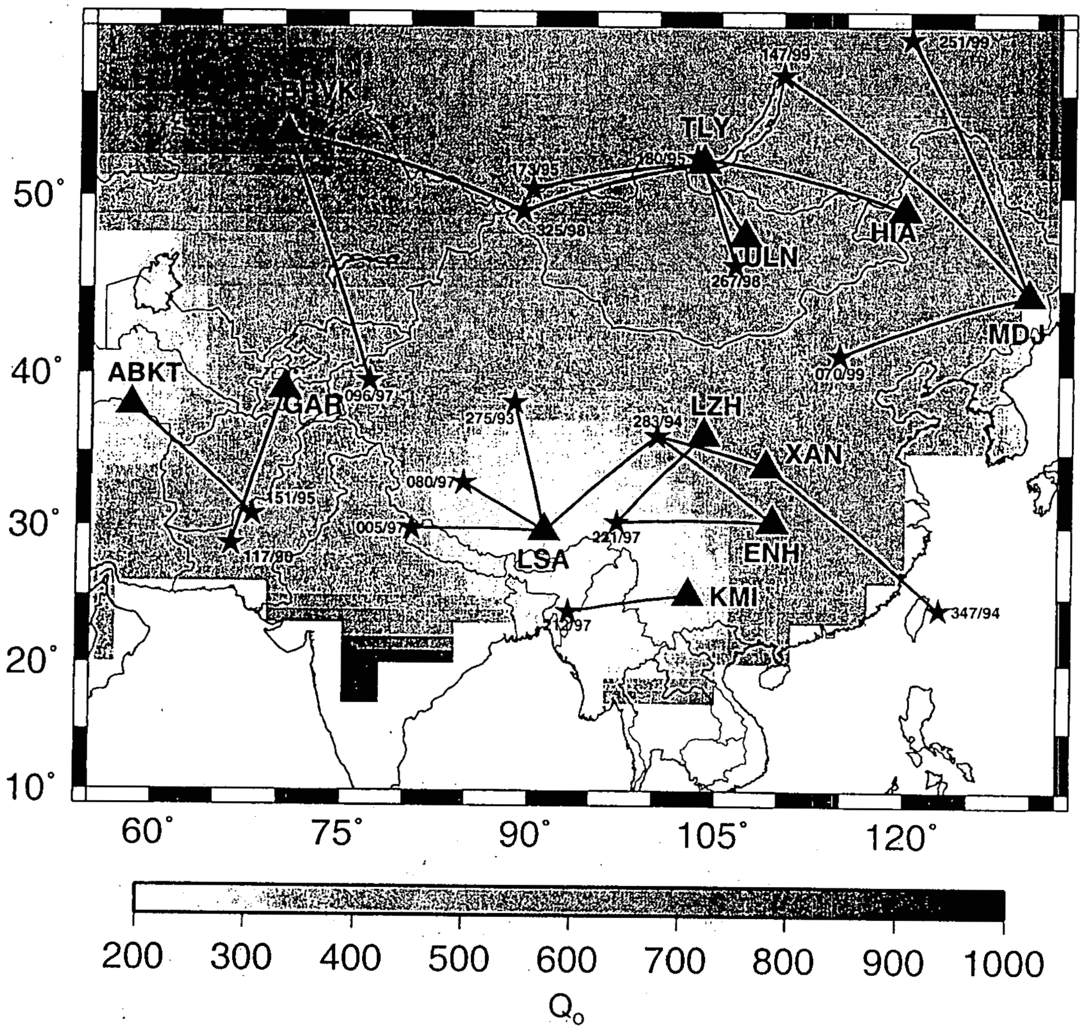
BRVK
TLY
HIA
ULN
MDJ
ABKT
GAR
LZH
XAN
ENH
LSA
KMI
50°
40°
30°
20°
10°
60°
75°
90°
105°
120°
200
300
400
500
600
700
800
900
1000
Q_o

Figure 5

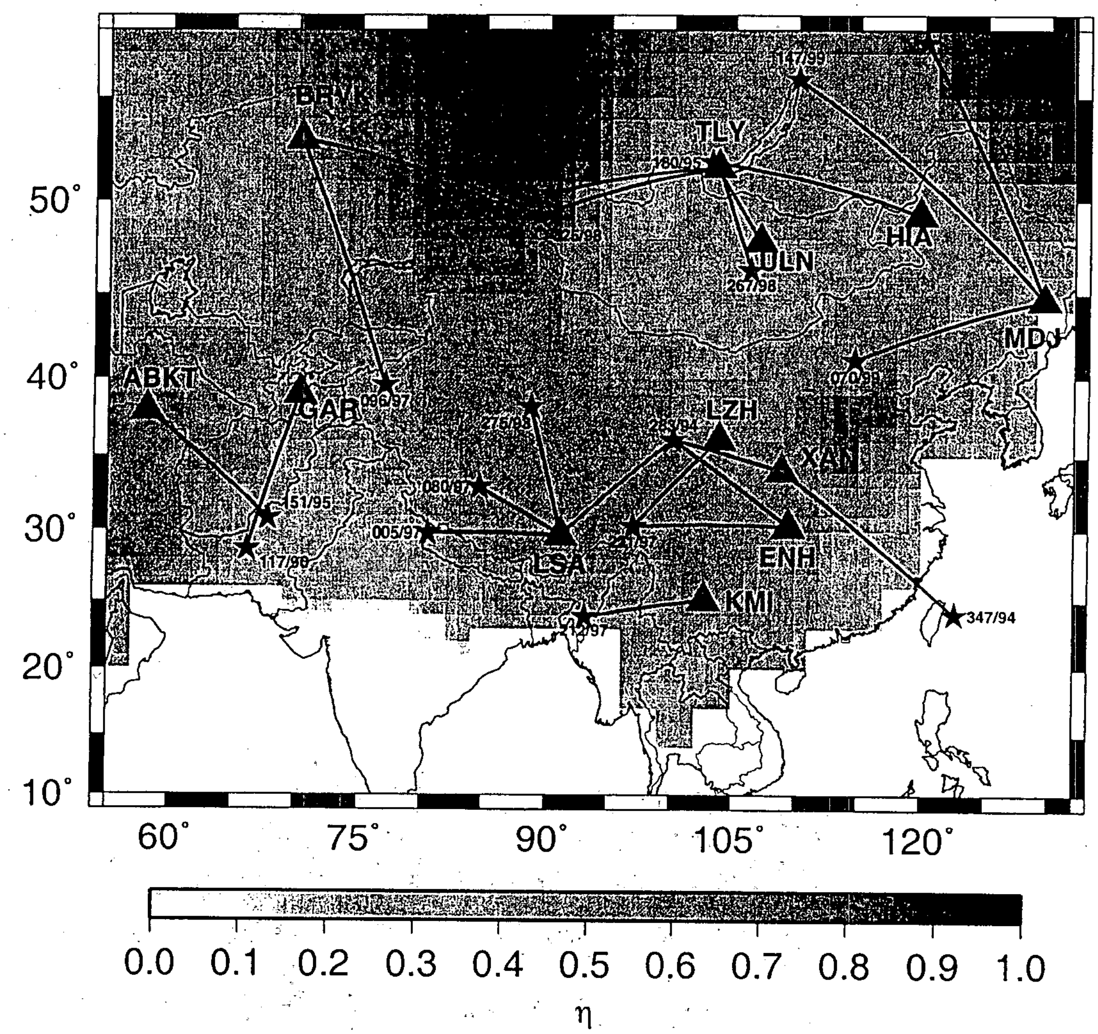
BRVK
TLY
180/95
HIA
ULN
267/98
MDJ
070/98
ABKT
GAR
096/97
275/97
LZH
XAN
080/97
151/95
005/97
LSA
ENH
117/98
KMI
347/94
50°
40°
30°
20°
10°
60°
75°
90°
105°
120°
0.0
0.1
0.2
0.3
0.4
0.5
0.6
0.7
0.8
0.9
1.0
η

Figure 6

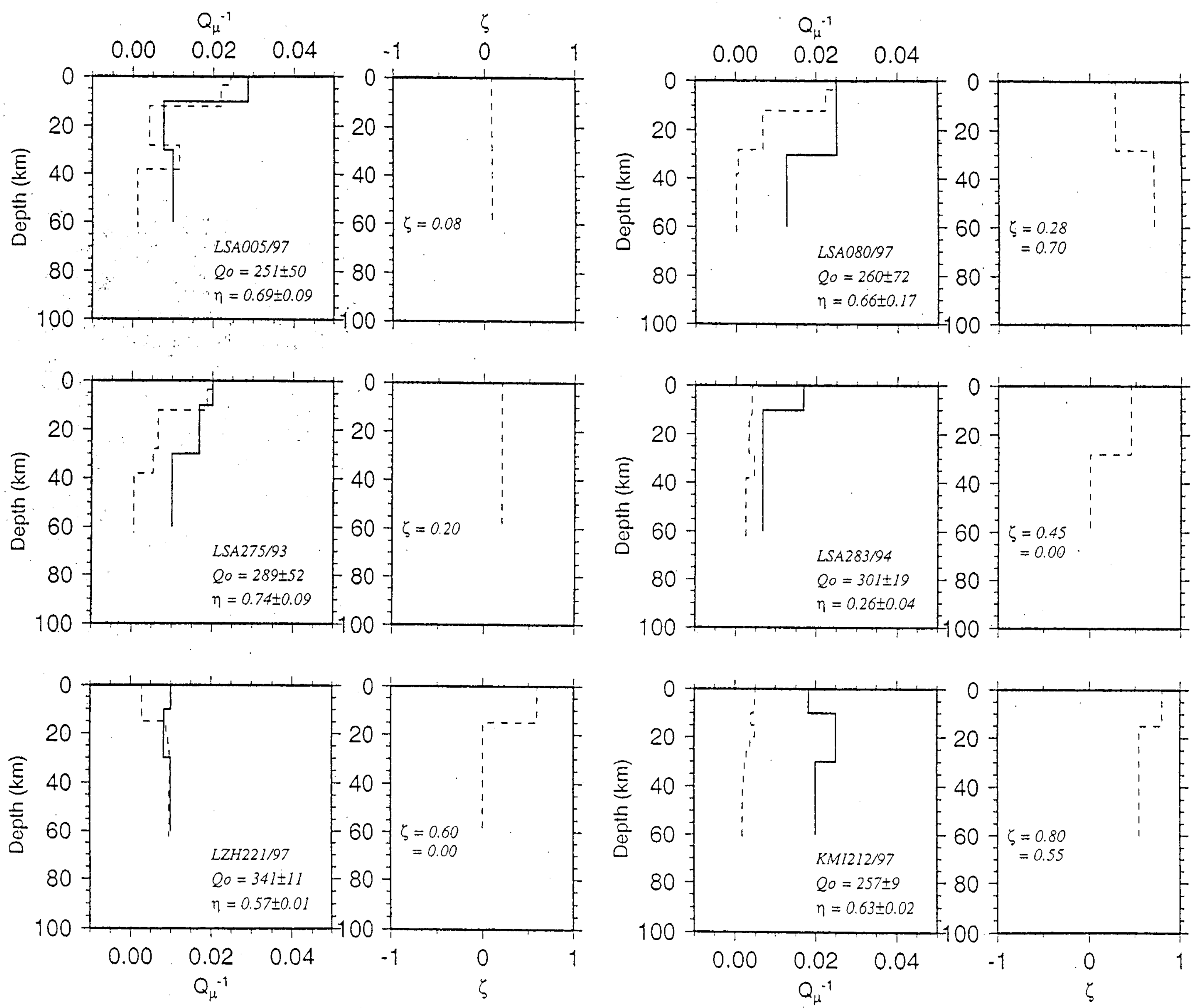

LSA005/97
Qo = 251±50
η = 0.69±0.09
ζ = 0.08
LSA080/97
Qo = 260±72
η = 0.66±0.17
ζ = 0.28
= 0.70
LSA275/93
Qo = 289±52
η = 0.74±0.09
ζ = 0.20
LSA283/94
Qo = 301±19
η = 0.26±0.04
ζ = 0.45
= 0.00
LZH221/97
Qo = 341±11
η = 0.57±0.01
ζ = 0.60
= 0.00
KMI212/97
Qo = 257±9
η = 0.63±0.02
ζ = 0.80
= 0.55
Depth (km)
Qμ-1
ζ

Figure 7a

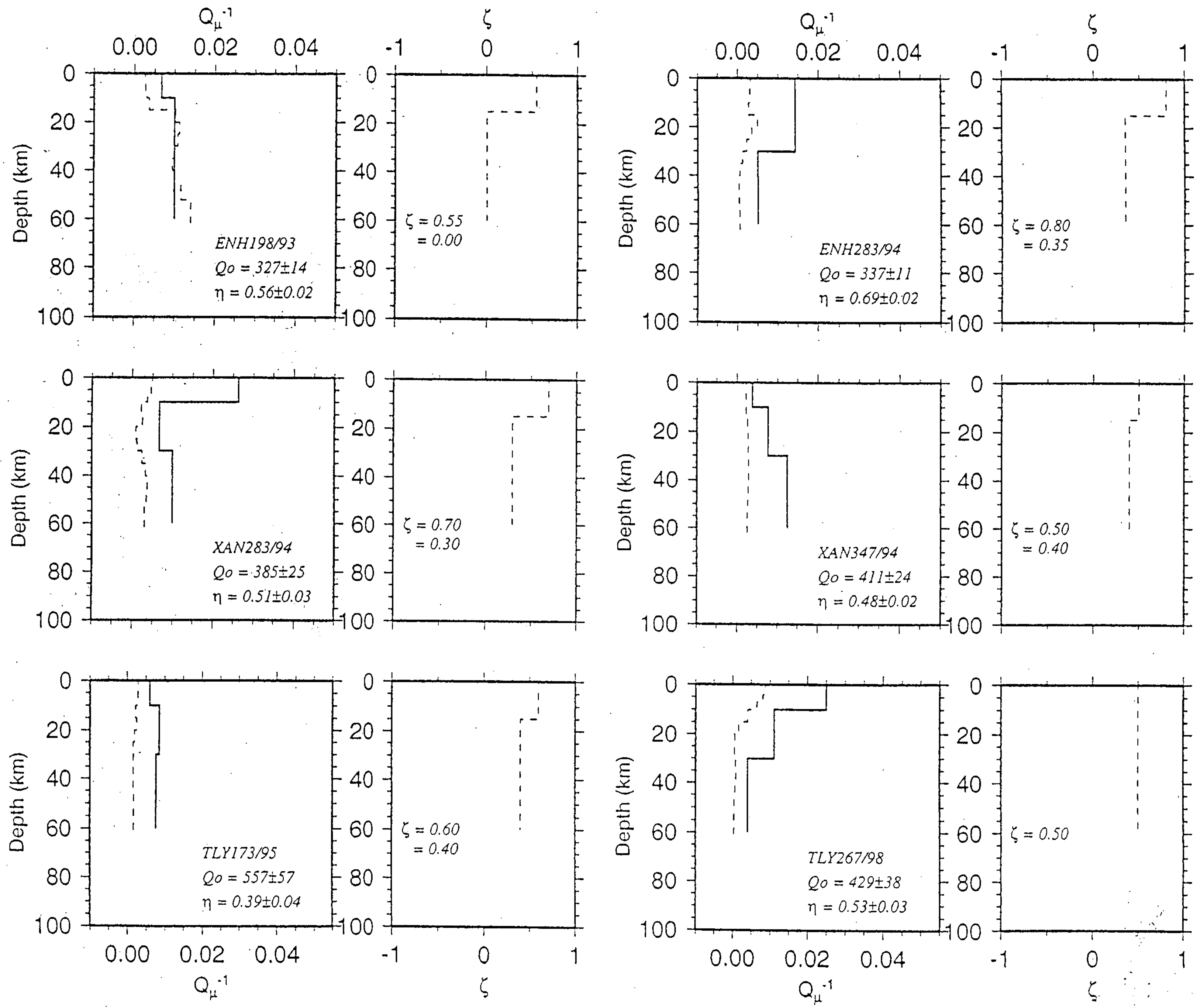

ENH198/93
Qo = 327±14
η = 0.56±0.02
ζ = 0.55
= 0.00
ENH283/94
Qo = 337±11
η = 0.69±0.02
ζ = 0.80
= 0.35
XAN283/94
Qo = 385±25
η = 0.51±0.03
ζ = 0.70
= 0.30
XAN347/94
Qo = 411±24
η = 0.48±0.02
ζ = 0.50
= 0.40
TLY173/95
Qo = 557±57
η = 0.39±0.04
ζ = 0.60
= 0.40
TLY267/98
Qo = 429±38
η = 0.53±0.03
ζ = 0.50
Depth (km)
Qμ-1
ζ

Figure 7b

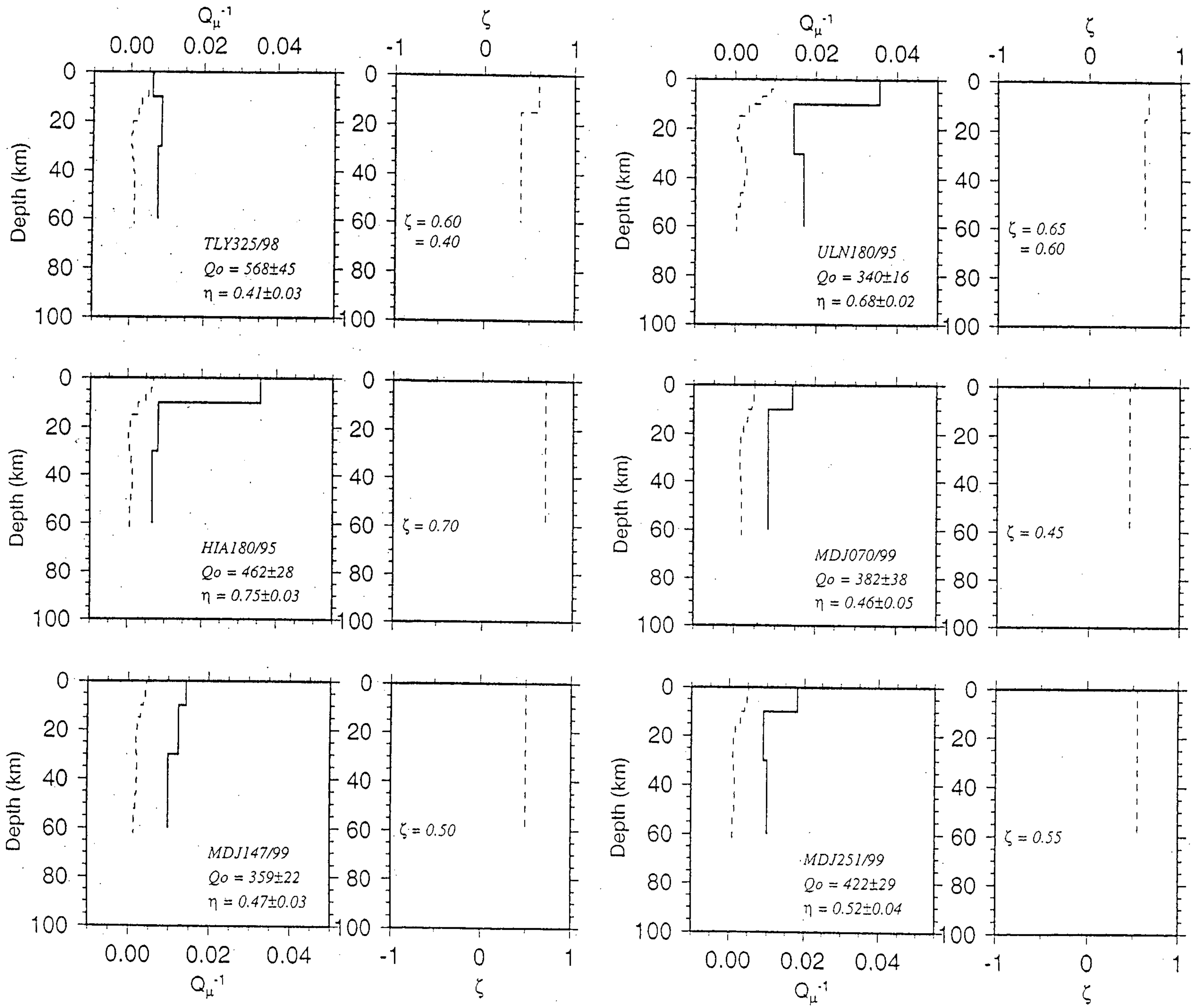

TLY325/98
Qo = 568±45
η = 0.41±0.03
ζ = 0.60
= 0.40
ULN180/95
Qo = 340±16
η = 0.68±0.02
ζ = 0.65
= 0.60
HIA180/95
Qo = 462±28
η = 0.75±0.03
ζ = 0.70
MDJ070/99
Qo = 382±38
η = 0.46±0.05
ζ = 0.45
MDJ147/99
Qo = 359±22
η = 0.47±0.03
ζ = 0.50
MDJ251/99
Qo = 422±29
η = 0.52±0.04
ζ = 0.55
Depth (km)
Q_μ^{-1}
ζ

Figure 7c

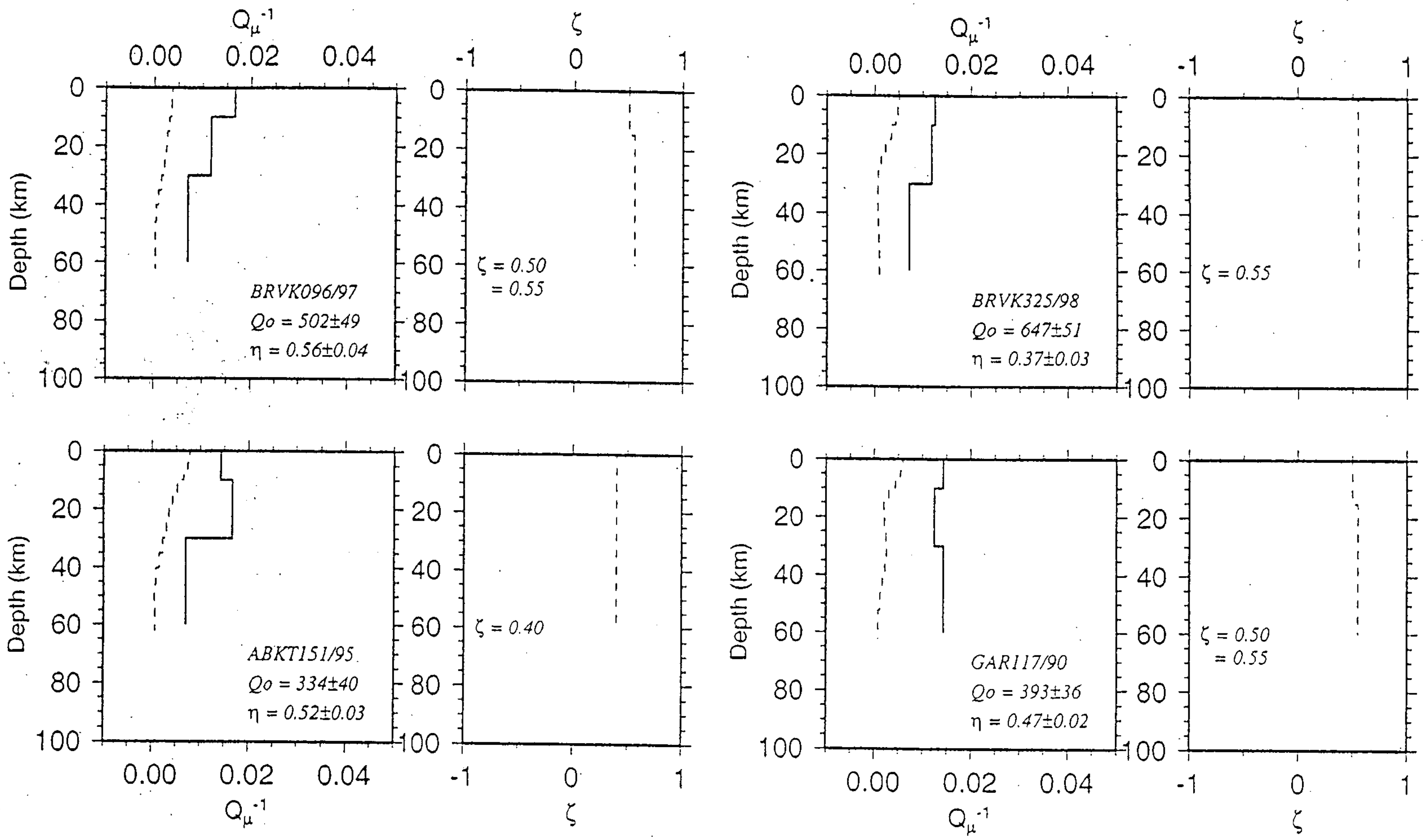
BRVK096/97
Qo = 502±49
η = 0.56±0.04
ζ = 0.50
= 0.55
BRVK325/98
Qo = 647±51
η = 0.37±0.03
ζ = 0.55
ABKT151/95
Qo = 334±40
η = 0.52±0.03
ζ = 0.40
GAR117/90
Qo = 393±36
η = 0.47±0.02
ζ = 0.50
= 0.55
Depth (km)
Qμ-1
ζ

Figure 7d

Computational Study of High-frequency P-wave Synthetics and their Attenuation in Continental Crust

F. Leyton, R. Chu, A. Fatehi and B.J. Mitchell
Department of Earth and Atmospheric Sciences
Saint Louis University

Abstract

We have completed preliminary studies of the effect that simple velocity and Q models have on the attenuation of high-frequency P-waves for distances between 10 and 200 km from a source in the upper crust. We computed complete waveforms that might propagate in simple high- and low-Q crustal models, one corresponding to a typical stable region and the other to a low-Q model that approximates a portion of a region of plate collision in China. Both models consist of a 10-km thick upper crustal layer over a half-space. Amplitudes were determined as a function of distance by computing record sections of complete waveforms using a wave-number integration code. The computed seismograms show that the rate of attenuation with distance is much more rapid for the low-Q model than for the high-Q model at the higher frequencies but only slightly more rapid at 1-Hz. Record sections show that the maximum amplitudes occur at epicentral distances somewhat smaller that the critical distance for the model we used. Maximum amplitudes for waveforms that have been band-pass filtered at 1, 3 and 5 Hz shift to lower frequencies with decreasing distance. Our computations show that the value selected for the frequency-dependence parameter (ζ) will have a very large effect on the computed amplitudes. For vertical-component ground motion our selected ζ value (0.5) yields maximum amplitudes at 5 Hz that are about 4 times as large as those at 1 Hz and 1.5 times as large as those at 3 Hz. Computations of horizontal-component ground motion yield similar results.

Introduction

Studies of seismic-wave attenuation have, over that past 20-30 years, greatly enhanced our understanding of the anelastic properties of the crust and upper mantle at surface-wave frequencies (~0.01-0.2 Hz) as well as for some waves at higher frequencies, such as Lg and its coda near 1 Hz. Much less is known about the attenuation of seismic waves frequencies higher than 1 Hz. These waves have, however, taken on greater importance as test-ban monitoring programs attempt to use shorter paths than ever before in order to detect and locate small events and to distinguish them from earthquakes.

We need to study the attenuation of these phases if we are to understand all facets of Q and its frequency dependence over broad frequency ranges. The purpose of this section of our report is to describe preliminary results obtained from the computation of P-wave synthetics for simple velocity and Q models that might be characterized by reasonable values for velocity and Q at relatively high frequencies (1–10 Hz).

We computed waveforms for direct P-waves using a wave-number integration code developed at Saint Louis University and MIT by B. Mandal (Mandal and Mitchell, 1986; Mandal and Toksöz, 1990). While the early codes synthesized complete waveforms for the specialized case of transverse isotropy with a vertical axis of symmetry, the more recent codes perform those computations for waves traversing generalized (up to 21 elastic constants) anisotropic media. While we have performed several types of computation, some with the intention of investigating the possibility of anisotropic Q in the continental crust, the present application restricts computations to wave propagation in isotropic media.

We consider our computations to be preliminary but they have yielded results suggesting that knowledge of high-frequency wave attenuation will be an important area for future research directed toward monitoring a comprehensive nuclear-test-ban treaty or CTBT.

High-frequency P-wave Attenuation for High-Q and Low-Q Crustal Models

In order to try to understand the attenuation of high-frequency (above 1 Hz) P-waves we restricted our computations in these preliminary computations to direct waves at relatively short distances. We constructed record sections for direct P-waves generated by a 5-km deep source and that have traveled 200 km through simple two-layer models (Table 1). The upper layer is 10 km thick and has a P-velocity typical of granitic rock, with corresponding values for S-velocity and density.

For our computations we took two end-member cases, a high-Q model that might be representative of an old stable continental region and a low-Q model that might characterize crust in a zone of continent-continent collision such as that occurring in the Tethysides belt of southern Eurasia. We have based the low-Q model on values that might be expected for a portion of southern Asia in which Jemberie and Mitchell (2003) studied shear-wave Q variations using Rayleigh waves. For our computations we assume that P-wave Q is twice as high as S-wave Q for those models. These considerations give a high-Q P-wave model for which Q is 1000 in the upper 10 km of the model and 600 in the lower layer and a low-Q model with a P-wave Q value of 100 in the upper layer and 140 in the lower layer.

For all computations we assume a value for the frequency dependence parameter of Q (see part I of this report) to be 0.5. This value is a rough average of the upper crustal frequency-dependence parameters found by Jemberie and Mitchell (2003b) for the crust of southeastern Asia that includes China and surrounding regions. Our computational results are likely to depend strongly on the value of this parameter, so it will be important to determine its value and regional variation for frequency ranges that are important in test ban monitoring.

After computing the P waveform at each distance, we filtered the trace with narrow band-pass filters centered at 1 Hz, 3 Hz and 5 Hz. Record sections for these three cases appear in Figures 1, 2 and 3, each showing seismograms for both the high-Q and low-Q models. The record sections cover the distance range 10-200 km with a station spacing of 10 km. The apparent velocities of the computed wave indicate that they begin seeing the faster, deeper layer at distances between about 50 and 70 km.

Noise was not added to the seismograms, but it is clear that P-waves in the low-Q model would be difficult to detect in the presence of noise at all three frequencies at distances greater than about 150 km for small events and that the onsets are so emergent that they would not be useful for precise event location even at much shorter distances. The high-Q model produces records in which amplitudes attenuate much more slowly and could, at the higher frequencies, probably be detected at distances beyond 200 km if the noise level is not high. The sharpness of the wave onsets for the high-Q model also makes those waves more useful for event location.

Figure 4 plots vertical-component P-wave amplitudes as a function of distance for the three frequencies for both our high- and low-Q models. For each frequency the amplitude maxima for the low- and high-Q models occurs at about the same distance, where that distance increases with decreasing frequency. Amplitude variations with distance show that 1-Hz waves have the largest amplitudes of the three frequencies at distances begin at about 70 km for the high-Q model and at about 65 km for the low-Q model. Amplitude for the 1-Hz waves are twice or more as large as for the other frequencies at all greater distances. At distances of 40-50 km the amplitudes of the 5-Hz waves are more than four times greater than the 1-Hz waves and about 1.5 times greater than the 3-Hz waves.

Similar distributions were obtained for the radial component of computed P-waves (Figure 5). Peak amplitudes of radial-component waves are higher than for the vertical-component, but this is only because of the constant velocity in the upper layer of the model. With a more realistic model in which velocities increase with depth the vertical-component amplitudes would become much larger than those obtained in this preliminary work.

Conclusions

Computations of vertical- and horizontal-component ground motion from a source at 5 km depth and an assumed value of 0.5 for the frequency dependency parameter in the upper crust have allowed us to determine the variation of P-wave amplitudes with distance in a simple two-layer model. Synthetic seismograms indicate that it may be difficult to detect small events at larger distances, especially if noise is present, for the low-Q model and that emergent waveforms, especially at 1 Hz, will degrade attempts to locate the events over a large distance range. At higher frequencies (3 and 5 Hz) the onsets are sharper, thus yielding better locations, but the waves attenuate very rapidly for the low-Q relative to the high-Q model. Synthetics at the higher frequencies decay very rapidly for the low-Q model relative to the high-Q model whereas synthetics at 1 Hz show less difference for the model we have tested.

Amplitude maxima shift to larger distances with decrease in frequency. For our selected model amplitude maxima occur at distances of 45, 60 and 75 km for frequencies of 5, 3 and 1 Hz, respectively. Plotted amplitudes for the higher frequencies are large at distances near and inside the critical distance but fall off rapidly at distances greater than about 70 km. Selection of other values for the frequency dependence parameter are likely to produce far difference results for amplitude attenuation with distance for the high-frequency waves of this study. With our selected ζ value maximum amplitudes at 5 Hz are 4 times and 1.5 times greater than at 1 Hz and 3 Hz, respectively.

References

Jemberie, A.L., and B.J. Mitchell (2003a), Shear-wave Q structure and its lateral variation in the crust of China and surrounding regions, *Geophys. J. Int.*, submitted.

Jemberie, A.L., and B.J. Mitchell (2003b), Frequency-dependent shear-wave Q models for the crust of China and surrounding regions, *Pure Appl. Geophys.*, submitted.

Mandal, B., and B.J. Mitchell (1986), Complete seismogram synthesis for transervsely isotropic media, *J. Geophys.*, 59, 149-156.

Mandal, B., and M.N. Toksös (1990), Computation of complete waveforms in general anisotropic media – results from an explosion source in an anisotropic medium, *Geophys. J. Int.*, 103, 33-45.

Table Caption

Table 1. Velocity-Q models utilized for the computations of this study.

Figure Captions

Figure 1. Vertical-component seismograms bandpass filtered around 1 Hz.

Figure 2. Vertical-component seismograms bandpass filtered around 3 Hz.

Figure 3. Vertical-component seismograms bandpass filtered around 5 Hz.

Figure 4. Amplitude variation with distance of P-wave vertical-component ground motion at frequencies of 1, 3 and 5 Hz for high- and low-Q models.

Figure 5. Amplitude variation with distance of P-wave radial-component ground motion at frequencies of 1, 3 and 5 Hz for high- and low-Q models.

Table 1

		Layer 1	Layer 2
Thickness (km)		10	∞
P-wave vel. (km/s)		6.1	6.7
S-wave vel. (km/s)		3.1	3.7
Density (gm/cc)		3.5	3.8
Q_P	Low-Q model	100	140
	High-Q model	1000	600
Q_S	Low-Q model	50	70
	High-Q model	500	300

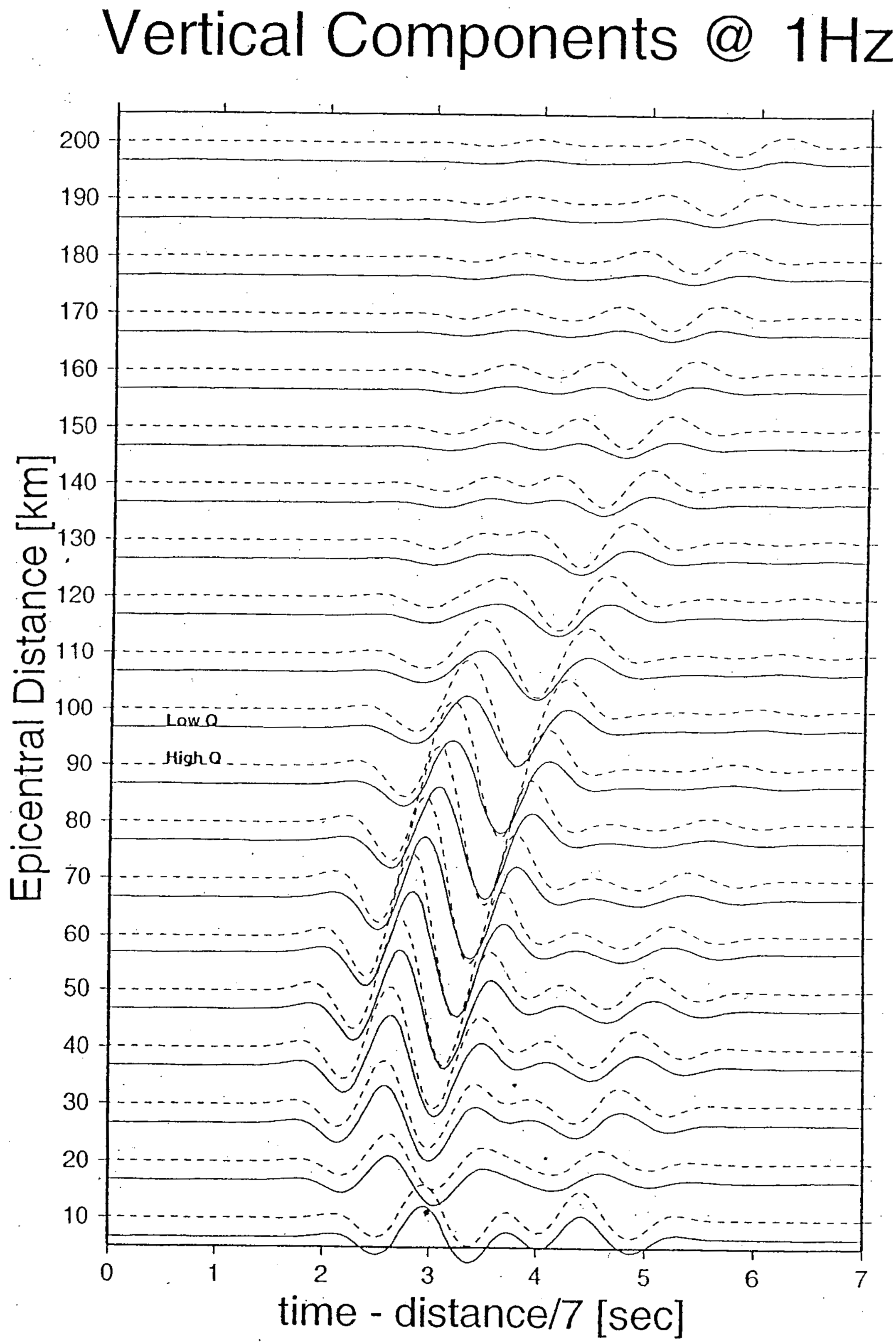
Vertical Components @ 1Hz
Epicentral Distance [km]
200
190
180
170
160
150
140
130
120
110
100
90
80
70
60
50
40
30
20
10
Low Q
High Q
0
1
2
3
4
5
6
7
time - distance/7 [sec]

Figure 1

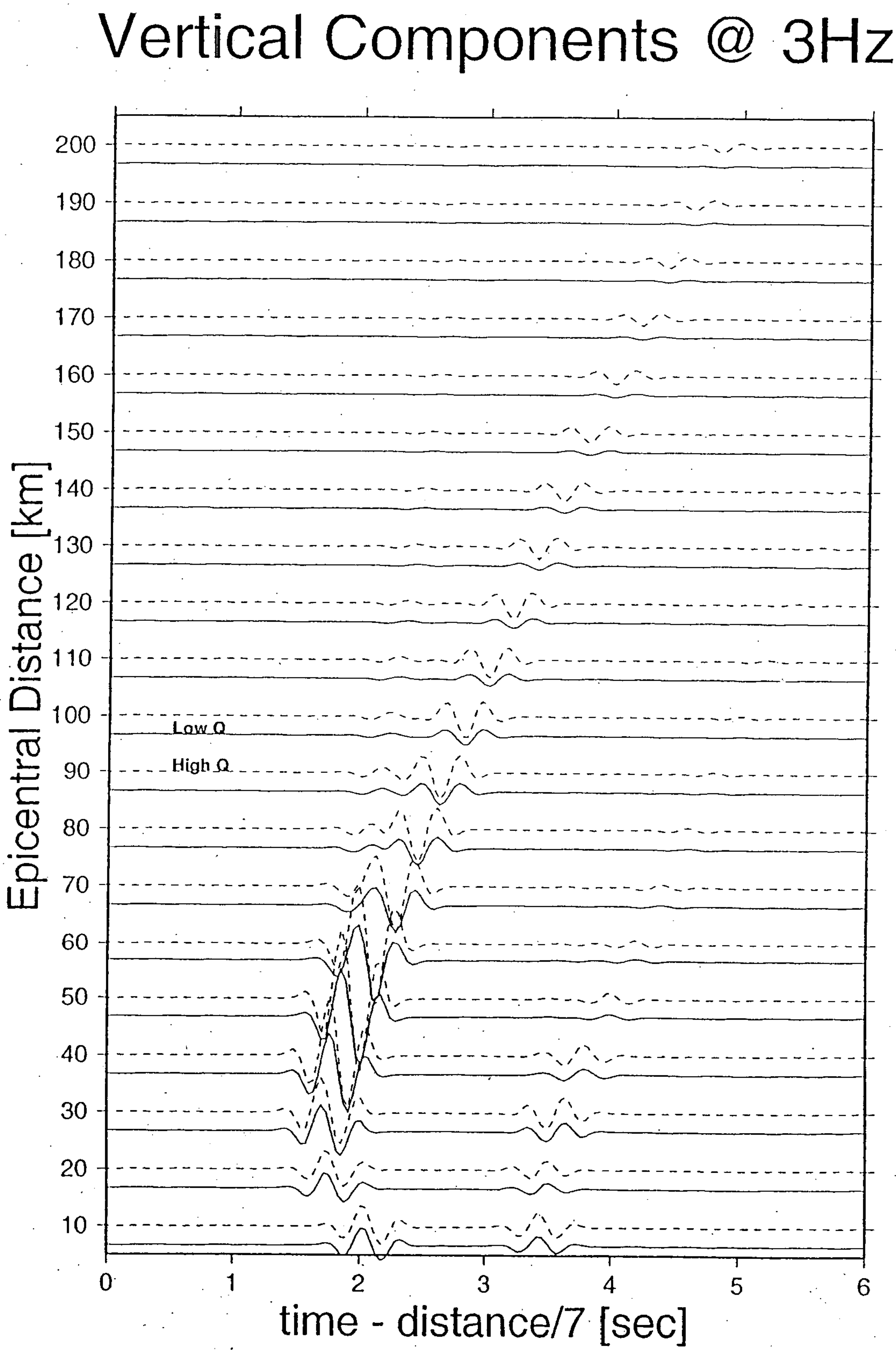
Vertical Components @ 3Hz
Epicentral Distance [km]
200
190
180
170
160
150
140
130
120
110
100
90
80
70
60
50
40
30
20
10
Low Q
High Q
0
1
2
3
4
5
6
time - distance/7 [sec]

Figure 2

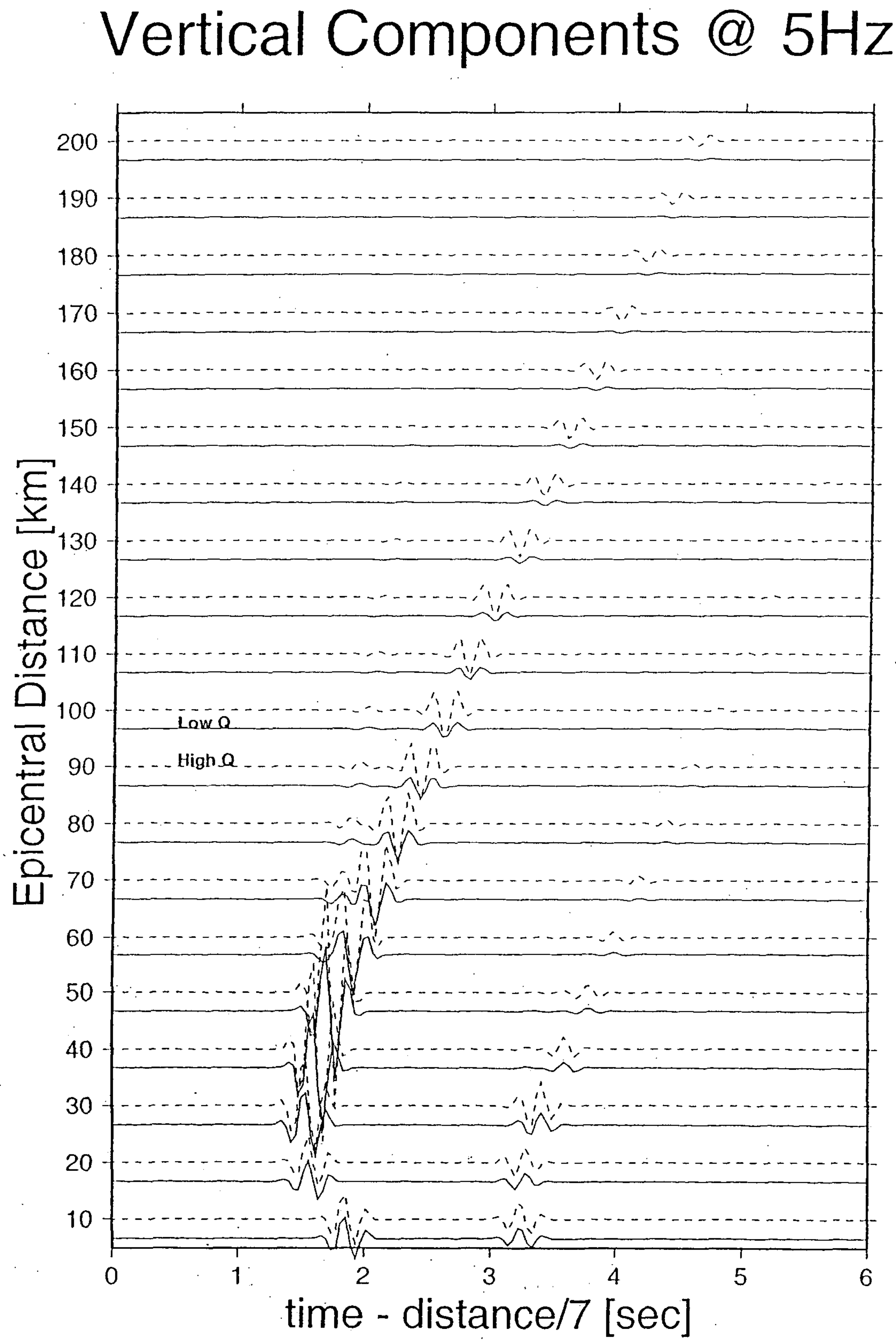
Vertical Components @ 5Hz
Epicentral Distance [km]
200
190
180
170
160
150
140
130
120
110
100
90
80
70
60
50
40
30
20
10
Low Q
High Q
0
1
2
3
4
5
6
time - distance/7 [sec]

Figure 3

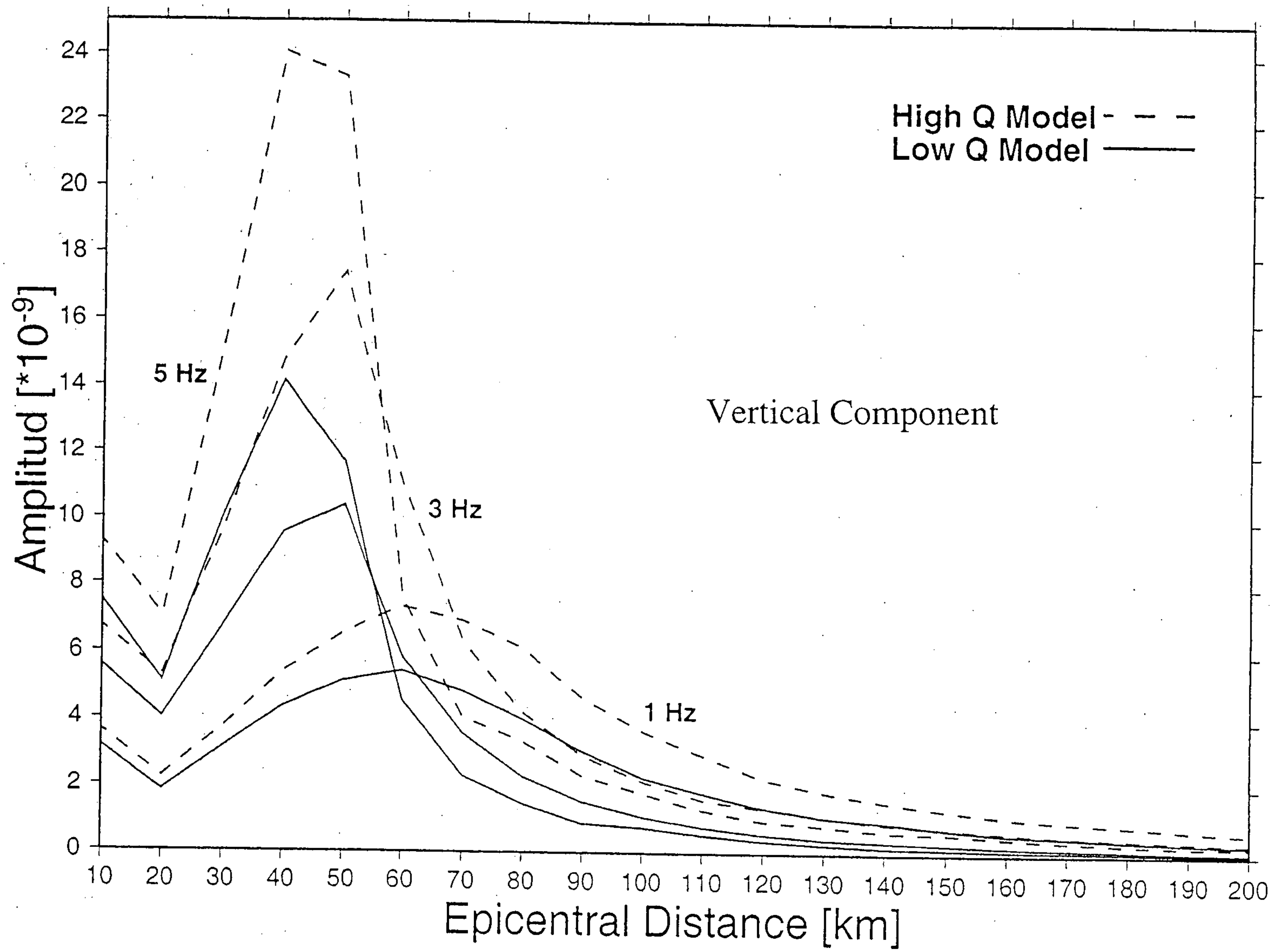
High Q Model
Low Q Model
Vertical Component
5 Hz
3 Hz
1 Hz
Amplitud [*10-9]
Epicentral Distance [km]
0
2
4
6
8
10
12
14
16
18
20
22
24
10
20
30
40
50
60
70
80
90
100
110
120
130
140
150
160
170
180
190
200

Figure 4

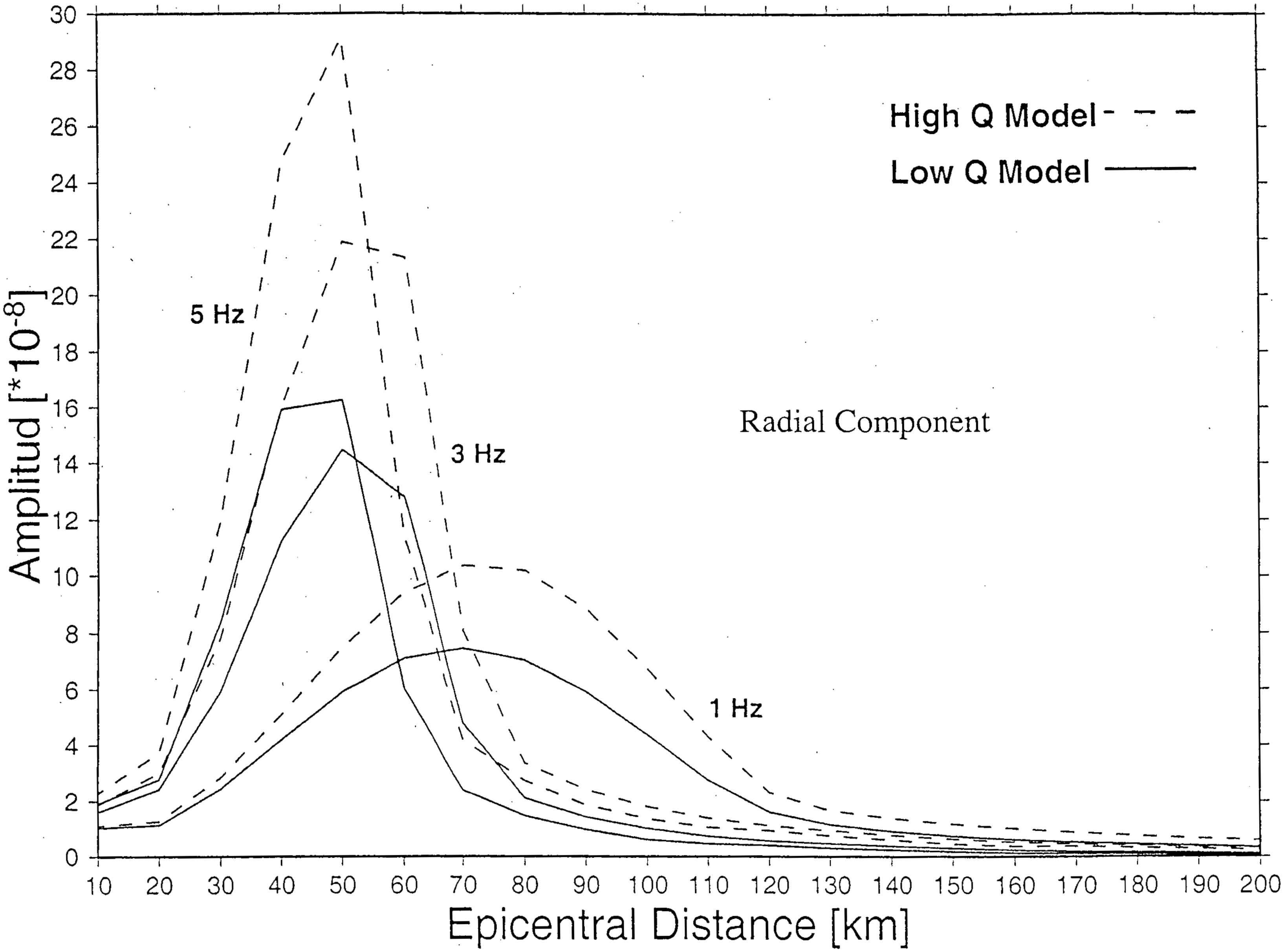
High Q Model
Low Q Model
5 Hz
3 Hz
1 Hz
Radial Component
Amplitud [*10^-8]
Epicentral Distance [km]
0
2
4
6
8
10
12
14
16
18
20
22
24
26
28
30
10 20 30 40 50 60 70 80 90 100 110 120 130 140 150 160 170 180 190 200

Figure 5

DISTRIBUTION LIST
DTRA-TR-03-31

DEPARTMENT OF DEFENSE

DEFENSE TECHNICAL INFORMATION CENTER
8725 JOHN J. KINGMAN ROAD,
SUITE 0944
FT. BELVOIR, VA 22060-0944
2 CYS ATTN: DTIC/OCA

DEFENSE THREAT REDUCTION AGENCY
8725 JOHN J. KINGMAN ROAD MS 6201
FT. BELVOIR, VA 22060-6218
2 CYS ATTN: TDND/ D. BARBER

DEPARTMENT OF DEFENSE CONTRACTORS

ITT INDUSTRIES
ITT SYSTEMS CORPORATION
1680 TEXAS STREET, SE
KIRTLAND AFB, NM 87117-5669
2 CYS ATTN: DTRIAC
ATTN: DARE

SAINT LOUIS UNIVERSITY
DEPARTMENT OF EARTH AND ATMOSPHERIC
SCIENCES
ST. LOUIS, MO 63103
ATTN: B.J. MITCHELL